



Università Campus Bio-Medico di Roma

Corso di dottorato di ricerca in
Scienze Biomediche Integrate e Bioetica.

XXXII ciclo a.a. 2016-2017

**Raman Spectroscopy into thyroid nodular pathology:
from bench to clinical application**

Isabella Giovannoni

Coordinatore
Prof. Paolo Pozzilli

Tutori
Prof. Paolo Pozzilli
Dr.ssa Anna Crescenzi

09 Luglio 2020

Tesi di dottorato in Scienze biomediche integrate e bioetica, di Isabella Giovannoni,
discussa presso l'Università Campus Bio-Medico di Roma in data 9/07/2020.
La disseminazione e la riproduzione di questo documento sono consentite per scopi di didattica e ricerca,
a condizione che ne venga citata la fonte.

A handwritten signature in black ink, consisting of a stylized initial followed by a horizontal line.

1. Background

1.1. Thyroid cancer

1.1.1. Classification

1.1.2. Incidence

1.1.3. Diagnostic Criteria

1.1.4. Molecular testing in thyroid cancer

1.2. Raman Spectroscopy

1.2.1. Raman technique

1.2.2. Role of Raman spectroscopy for cancer diagnosis

1.2.3. Raman spectroscopy in thyroid cancer

1.2.4. Limitation of Raman spectroscopy

2. Purpose

3. Material and Methods

4. Results and Discussion

5. Conclusion

6. References



Abbreviations


AHCA	agglomerative hierarchical clustering analysis
APC	annual percentage change
ATC	anaplastic thyroid carcinoma
AUS/FLUS	atypia of undetermined significance/follicular lesion of undetermined significance
CT	serum calcitonin
DTC	differentiated thyroid cancer
ECACC	European Collection of Cell cultures
FC	follicular thyroid carcinoma
FMTC	familial medullary thyroid carcinoma
FN/SFN	follicular neoplasm/suspicious for neoplasm
FNA	Fine needle aspiration
FNAC	Fine needle aspiration cytology
FV-PTC	follicular variant of papillary carcinoma
GEC	Afirma® Gene Expression Classifier
IHC	immunohistochemistry
KM	K-means
MEN2A	multiple endocrine neoplasia 2A
MEN2B	multiple endocrine neoplasia 2B
MTC	Medullary thyroid carcinoma
NGS	next-generation sequencing
NPV	negative predictive value
PCA	Principal Component analysis
PPV	positive predictive value
PTC	papillary thyroid carcinoma
RS	Raman spectroscopy
SERS	Surface-Enhanced Raman Scattering
SORS	Spatially offset Raman spectroscopy
TCGA	The Cancer Genome Atlas
Tg	thyroglobulin
TSH	thyroid stimulating hormone
UCBM	University of Campus Bio-Medico
US	ultrasound



1. Background

1.1 Thyroid cancer

The incidence of thyroid cancer continues to rise worldwide, mostly as a result of increased use of diagnostic imaging and surveillance. Thyroid cancer estimated over 62000 new cases occurred in men and women in 2015 (Cabanillas, McFadden et al. 2016). Although incidence is rising steadily, mortality from thyroid cancer has changed minimally over the past five decades. The challenge faced by physicians who treat thyroid cancers is to balance the therapeutic approach so that patients with lower risk disease or benign thyroid nodules are not over treated. At the same time, they need to recognize those patients with more advanced or high-risk disease, which need a more aggressive treatment approach. Thyroid cancers exhibit a broad range of clinical behavior - from indolent tumors with low mortality in most cases, to very aggressive malignancies, for example, anaplastic thyroid cancer. Therefore, undertaking a proper diagnostic workup before treatment is started is crucial to appropriately tailor treatment.



1.1.1 Classification

Thyroid carcinomas are classified according to the cell type they derive from, their degree of differentiation and their cytoarchitecture. Most primary thyroid cancers are epithelial tumors that originate from thyroid follicular cells. These cancers develop three main pathological types of carcinomas: papillary thyroid carcinoma (PTC), follicular thyroid carcinoma (FC), and anaplastic thyroid carcinoma (ATC). Medullary thyroid carcinoma (MTC) arises from thyroid parafollicular (C) cells.

The main histologic types of thyroid carcinoma are divided in:

1. Differentiated (PTC, FTC).
2. Medullary (MTC)
3. Anaplastic (ATC)

PTC and FC are categorized as differentiated thyroid cancer (DTC) because of well differentiation and indolent tumor growth. PTC consists of 85-90% of all thyroid cancer cases, followed by FC (5-10%) and MTC (about 2%). ATC accounts for less than 2% of thyroid cancers and typically arises in the elder patients.

Papillary thyroid carcinoma (PTC)

PTC is a major differentiated adenocarcinoma, which consists of 90% of thyroid cancers and shows papillary proliferation pathologically. Most cases have excellent prognosis but approximately 10% of PTC patients undergo recurrences such as lymph node recurrence and lung metastasis. Selecting such high-risk patients is the most important challenge as well as treatment of radioiodine refractory PTC.



Clinicopathologically, age>45 years, large tumor size, extra thyroidal invasion, distant metastasis, vascular invasion and poor differentiated histology are well known detrimental prognostic factors (DeLellis RA, Lloyd RV et al. 2004).

PTC is usually gray-white color and shows a variety of gross appearance such as tumors with central scar and infiltrative borders, encapsulated tumor and lesional calcification (Figure 1A). Nearly half of PTCs have multifocal lesions and regional lymph node metastasis. These characteristics do not affect long-term survival (Shaha, Loree et al. 1995).

Most of PTCs shows papillary growth pattern but nuclear features are more important diagnostic hallmark, which are common in almost all cases than such growth pattern itself (Figure 1B). The nuclear appearances of PTC are clear, ground glass, or Orphan-Annie eyed (Hapke and Dehner 1979). These nuclei are larger than normal follicular nuclei and overlapping each other. The nuclei contain eosinophilic inclusions and have longitudinal grooves (Scopa, Melachrinou et al. 1993). These nuclear features are important characteristics of PTC but not specific. Indeed, chronic thyroiditis frequently shows similar intranuclear inclusions or nuclear grooves as well as follicular adenoma (DeLellis RA, Lloyd RV et al. 2004).

Several subtypes are thought to be associated with either favorable or aggressive phenotype although it is still controversial. The most common variants are follicular variant, tall cell variant, diffuse sclerosis variant, and solid variant.

A certain part of follicular variant of papillary carcinoma (FV-PTC) was classified as FC or follicular adenoma in the past. The nuclei of this variant rarely have all of the features of PTC (eg. rare nuclear groove). Accordingly, FV-PTCs are often



diagnosed as indeterminate cytology in contrast to high diagnostic accuracy of usual PTC. FV-PTC is recognized by its follicular structure with papillary cytology, and composed of 2 subtypes; diffuse/invasive (infiltrative) and encapsulated type. FV-PTC is associated with favorable prognosis especially if tumor is encapsulated (Tielens, Sherman et al. 1994). Diffuse/invasive subtype has similar clinical features to usual PTC. Diagnosis of encapsulated subtype is still under debate since this subtype shows no invasion or incomplete nuclear characteristics. This encapsulated subtype is slowly growing and conservative treatment may be warranted (Liu, Singh et al. 2006).

Tall cell variant composes 10% of PTC, and have a 10-year mortality rate of up to 25%, less favorable prognosis than usual PTC. This variant is often associated with poor prognostic characteristics such as elder age, extra thyroidal invasion, and high mitotic rate. The tall cells are twice as tall as its width, and should occupy >50% of papillary carcinoma cells (DeLellis RA, Lloyd RV et al. 2004).

The diffuse sclerosis variant is 3% of PTC, which infiltrates the entire thyroid gland and is associated with younger age (Sherman 2003). Presence of many psammoma bodies is one of hallmarks of this variant. Extensive calcification causes exceedingly firm tumor. Background thyroid of this variant shows chronic lymphatic thyroiditis with lymphocytic infiltration, resembling Hashimoto disease (Chan, Tsui et al. 1987). This variant PTC often shows extra thyroidal extension and regional lymph node metastasis at diagnosis leading to decreased recurrence free survival although mortality is low (Fukushima, Ito et al. 2009).



Solid variant PTC is diagnosed when solid growth represents more than 50% of tumor. This variant is commonly seen in children and often associated with secondary PTC patients after the Chernobyl nuclear accident (Nikiforov, Gnepp et al. 1996). Both lymphatic and venous invasion are frequently observed in this variant (Nikiforov and Gnepp 1994). Some studies reported that the solid variant is associated with poor prognosis whereas others considered the prognosis of this variant is almost as good as usual PTC (Nikiforov, Gnepp et al. 1996, Collini, Mattavelli et al. 2006).

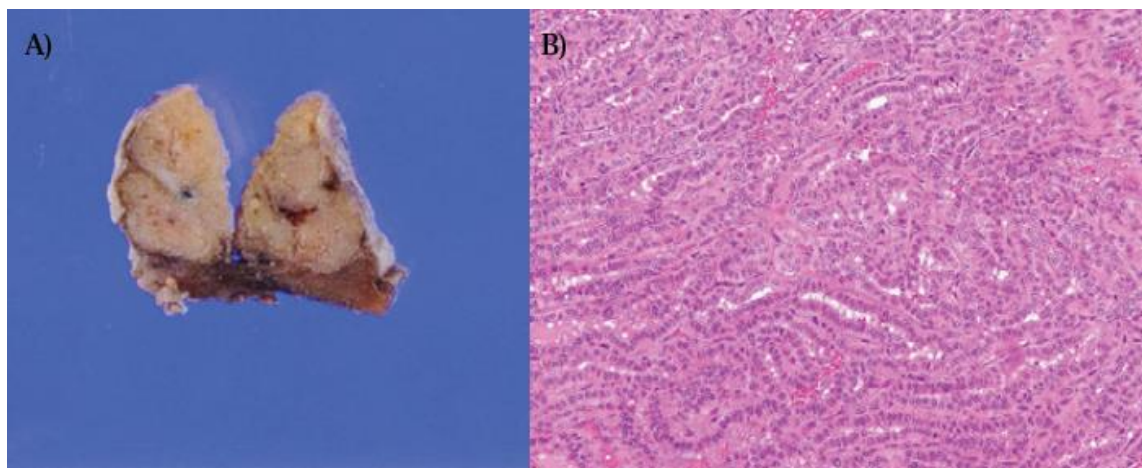
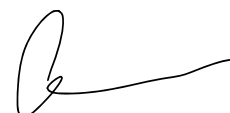


Fig. 1: Typical image of papillary thyroid carcinoma. Macroscopic (A) (scale bar = 10 mm) and microscopic (B) (H&E, x200) features of PTC

Follicular thyroid carcinoma (FC)

FC represents 5-15% of thyroid cancer with follicular differentiation but no papillary nuclear characteristics (DeLellis RA, Lloyd RV et al. 2004). FC is a solitary encapsulated tumor with gray-tan-pink color, usually focal hemorrhage. FC is diagnosed by follicular cell invasion of the tumor capsule and/or blood vessels.



Vascular invasion leads to worse prognosis than capsular infiltration alone (van Heerden, Hay et al. 1992). Majority of FCs are minimally invasive with slight tumor capsular invasion alone (Figure 2). These minimally invasive FCs are similar appearance to follicular adenomas and rarely cause distant metastasis (LiVolsi and Asa 1994). Accordingly, a minimally invasive FC is difficult to distinguish from a follicular adenoma in cytology or frozen section, and can be diagnosed only after thyroidectomy. Widely invasive FC is much less common but ~80% of these tumors cause distant metastasis, leading to high mortality rate at around 20%. The poor prognostic factors are distant metastasis, age>45 years, large tumor size, extensive vascular invasion, extra thyroidal extension, and widely invasive tumors (Ito, Hirokawa et al. 2007).

Hürthle cell carcinoma (oxyphilic cell carcinoma) is presumed to be a variant of FC but its prognosis is thought to be worse than usual FC (Sugino, Ito et al. 2001, Lopez-Penabad, Chiu et al. 2003). A variant of papillary carcinoma is rare and have similar prognosis as FC (Herrera, Hay et al. 1992). More than 75% follicular cells with oncocytic characteristics are included in Hürthle cell tumor (Stojadinovic, Ghossein et al. 2001). Oxyphilic or oncocytic cells are characterized by its polygonal shape, eosinophilic granular cytoplasm, hyper chromatic or vesicular nuclei with large nucleolus, and abundant mitochondria.



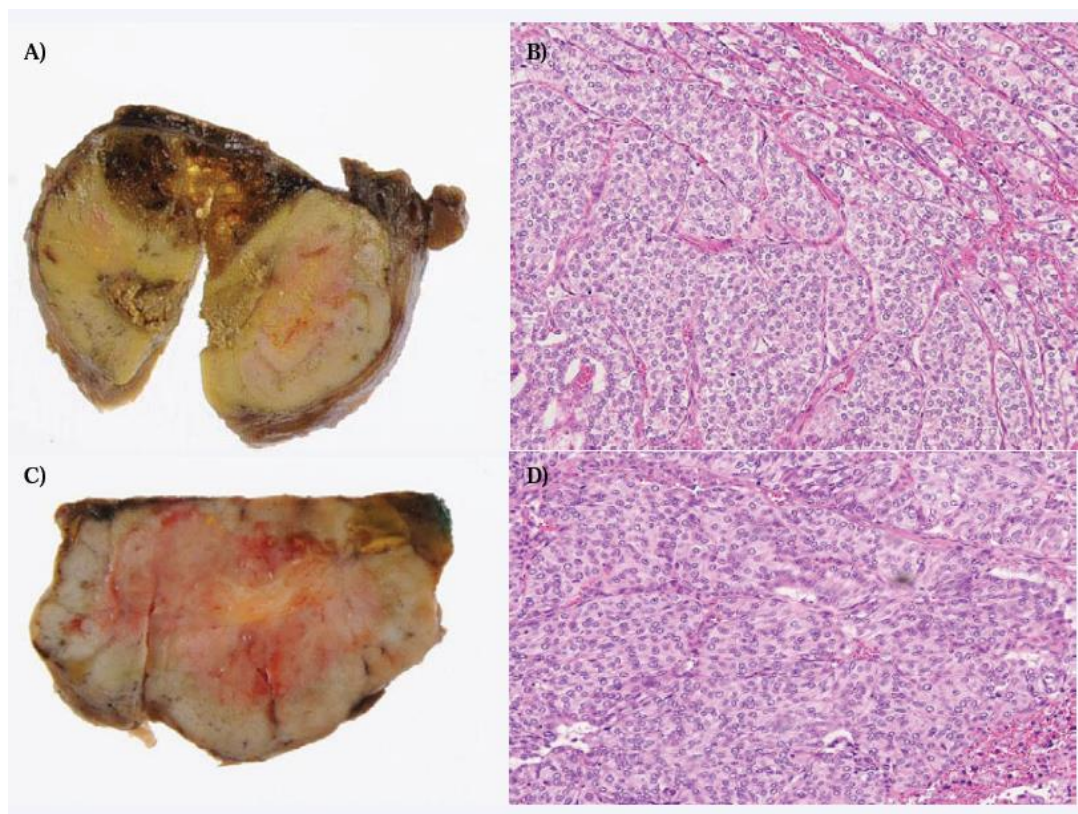


Fig. 2: Typical images of follicular thyroid carcinoma Macroscopic (A) (scale bar = 10 mm) and microscopic (B) (H&E, x200) images of minimally invasive (A and B) or widely invasive (C and D) FC.

Anaplastic thyroid carcinoma (ATC)

ATC is extremely aggressive undifferentiated tumor, with almost 100% disease-specific mortality (Are and Shaha 2006), representing about 40% thyroid cancer deaths by only <2% of thyroid cancers. The median survival from diagnosis is around 6 months (Untch and Olson 2006). ATC extensively invades into surrounding structures, and distant metastases are observed at diagnosis in one-third of ATC patients. Peak age of patients is older than that of DTCs and >70% of patients are women (Kebebew, Greenspan et al. 2005). Approximately 50% of ATC patients have prior or concurrent DTC. It is suggesting that ATC emerges as a result

A handwritten signature in black ink, consisting of a stylized initial 'G' followed by a long horizontal stroke.

of de-differentiation of DTC. In contrast to DTC, ATC usually does not uptake iodine, leading to refractoriness against radioiodine treatment. Although clinically apparent ATCs are usually unresectable, intrathyroidal ATCs are surgically resectable and such radical resection offers better outcomes (Sugitani, Hasegawa et al. 2014). ATC shows extremely invasive large solid tumor with necrosis and hemorrhage (Figure 3). Large, pleomorphic giant cells resembling osteoclasts is one of hallmarks of ATC cells (Gaffey, Lack et al. 1991). ATC is composed of spindle cells and squamoid cells.

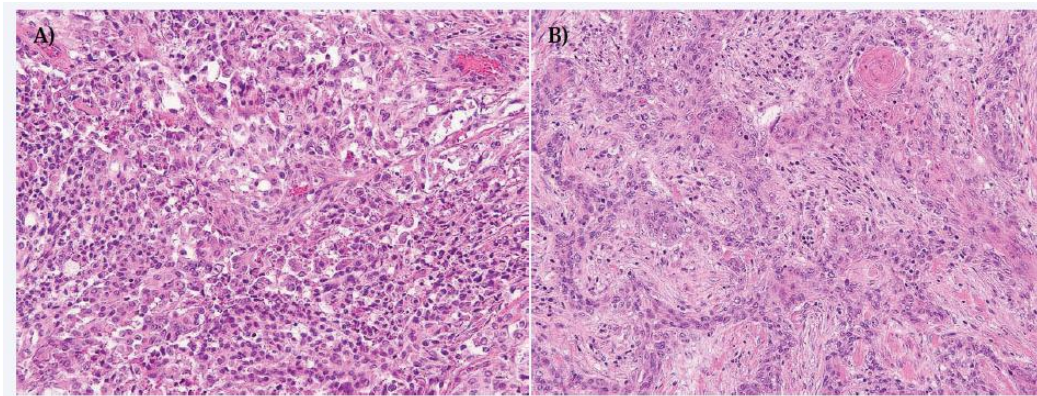


Fig. 3: Anaplastic thyroid carcinoma. Microscopic images of 2 cases of ATC (H&E, x200)

Medullary thyroid carcinoma (MTC)

MTC represents less than 5% of thyroid carcinomas, which is neuroendocrine tumor originated from C cells of ultimobranchial body of neural crest and secretes calcitonin. Seventy to eighty percent of MTCs are sporadic while 20-30% of MTCs are familial. Familial MTCs are all autosomal dominant inheritance of germ line RET mutations and classified to 3 categories; multiple endocrine neoplasia 2A



(MEN2A), multiple endocrine neoplasia 2B (MEN2B), and familial medullary thyroid carcinoma (FMTC) (Giuffrida and Gharib 1998). Peak age of familial MTC is younger (approximately 35 years) than of sporadic MTC (40-60 years). The overall 5-year survival of patients with MTC is 86%. Poor prognostic factors include older age, advanced stage, the presence of lymph node metastasis at diagnosis, and somatic *RET* mutation (Elisei, Cosci et al. 2008). Sporadic MTC is usually solitary whereas most of familial MTC exhibit bilateral, multicentric foci. MTCs typically exhibit gray-tan color, firm, solid tumors and do not have a well-formed capsule. Tumor includes high concentration of C cells. MTC cells are round to oval, spindle, or polyhedral. Broad fibrovascular bands separate tumors into nodules (Figure 4). The nuclei are round to oval with salt-and-pepper nuclear chromatin. Amyloid deposits from calcitonin are frequently present in stroma. A background of C cell hyperplasia is observed in familial but not in sporadic MTCs (Etit, Faquin et al. 2008).

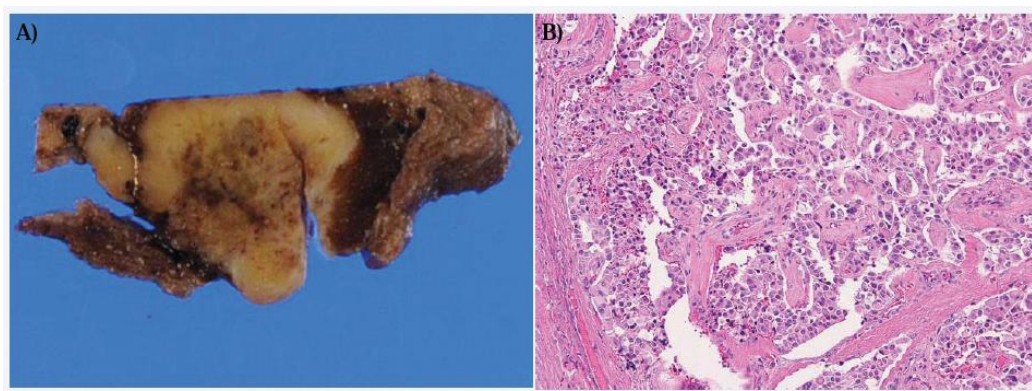


Fig. 4: Medullary thyroid carcinoma. Macroscopic (A) (scale bar = 10 mm) and microscopic (B) (H&E, x200) features of MTC

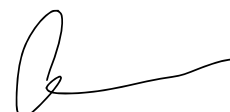
1.1.2 Incidence and risk factors for thyroid cancer

The annual incidence of thyroid cancer varies considerably by geographic area, age and sex. An average of 58.629 patients per year were diagnosed worldwide with thyroid carcinoma from 2008 to 2012. Of these 58.629 patients, 89% had papillary carcinoma, 5.1% had follicular carcinoma, 2.2% had Hürthle cell carcinoma, 1.7% had medullary carcinoma, and 0.8% had anaplastic carcinoma.

It is estimated that 64.300 new cases of thyroid cancer were predicted to be diagnosed in 2016 compared with 37,200 in 2009 when the last ATA guidelines. In the same year, approximately 1980 cancer deaths will occur among persons with thyroid carcinoma in the United States. Anaplastic carcinoma is almost uniformly lethal; however, most thyroid carcinoma deaths are from papillary, follicular and Hürthle cell carcinoma, which account from nearly 95% of all thyroid carcinoma cases (Siegel, Miller et al. 2016).

The yearly incidence has nearly tripled from 4.9 per 100,000 in 1975 to 14.3 per 100,000 in 2009. Almost the entire change has been attributed to an increase in the incidence of PTC. Moreover, 25% of the new thyroid cancers diagnosed in 1988–1989 were ≤ 1 cm compared with 39% of the new thyroid cancer diagnoses in 2008–2009 (Davies and Welch 2014).

The reported escalating incidence during the last decades all over the globe is mainly due to an increase in micropapillary (<2 cm) histotype, while there is no substantial change in the incidence of the less common histological categories: follicular, medullary and anaplastic cancers.



This tumor shift (>5% per year in both men and women) may be due to the increasing use of neck ultrasonography or other imaging and early diagnosis and treatment (Leenhardt, Bernier et al. 2004), trends that are changing the initial treatment and follow-up for many patients with thyroid cancer.

A recent population-based study from Olmsted County reported the doubling of thyroid cancer incidence from 2000 to 2012 compared to the prior decade as entirely attributable to clinically occult cancers detected incidentally on imaging or pathology (Brito, Al Nofal et al. 2015). Another recent study estimated that over the past 2 decades, about one-half of all papillary thyroid cancers diagnosed in women, and 40% of those in men aged ≤ 50 years, were clinically irrelevant (O'Grady, Gates et al. 2015).

It is common experience in thyroid cancer referral centers that nearly 60%–80% of thyroid carcinomas detected nowadays are micropapillary thyroid carcinomas (<1 cm in size) carrying an excellent long-term prognosis (Leenhardt, Bernier et al. 2004).

However, increases across tumor size and stage, as well as for follicular carcinoma (a more aggressive subtype), suggest that some of the rise may be due to changes in environmental risk factors, such as obesity (Aschebrook-Kilfoy, Grogan et al. 2013, Schmid, Ricci et al. 2015).

More recently, an increased incidence for all size of thyroid tumor has been reported in the USA. During 1997–2005, the annual percentage change (APC) for primary tumor <1.0 cm was 9.9 in man and 8.6 in women. A substantial increase was also observed for tumor >4 cm among men (1988–2005: APC 3.7) and women (1988–



2005: APC 5.7)(Chen, Jemal et al. 2009). These data suggested that increased diagnostic scrutiny is not the only explanation, and environmental influence should be considered.

The only established environmental risk factor for thyroid carcinoma is exposure to ionizing radiation, and the risk, particularly of papillary carcinoma, is greater in subjects of younger age at exposure. An increased incidence of thyroid cancer in children and adolescents was observed in Ukraine, Belarus and certain regions of Russia as early as 4 years after the Chernobyl accident. The pre-Chernobyl incidence of thyroid cancer in Ukrainian children was very low (0.5–1.0 per 1000000 children). Following the explosion of the Chernobyl nuclear reactor in 1986, a dramatic increase in the incidence of benign and malignant thyroid tumors (80 times more) was observed in children born or conceived around the time of the accident in a wide area surrounding the reactor (Tronko, Bogdanova et al. 1999). In addition to environmental factors, genetic factors are involved in thyroid cancer predisposition.


As previously mentioned, the increased incidence of thyroid cancer diagnoses has been attributed, in part, to improved detection of small or subclinical thyroid nodules on thyroid ultrasonography and by other imaging techniques; however, increased incidence of thyroid tumors of all sizes has also been reported. The increased number of cases of papillary thyroid cancer is predominantly of follicular variant, *RAS* mutation positive tumors, suggesting a potential role for environmental (chemical/dietary) factors(Jung, Little et al. 2014).



Aside from the well-characterized familial forms of medullary thyroid cancer, non-medullary thyroid cancer in a first-degree relative increases the risk 4-10 fold higher than in the general population (Frich, Glatte et al. 2001, Hemminki, Eng et al. 2005). Familial non-medullary thyroid cancer is characterized by autosomal dominant inheritance with reduced penetrance, and has been estimated to account for approximately 5-10% of all thyroid cancers (Mazeh and Sippel 2013). Genetic linkage studies have mapped susceptibility loci to several regions including 1q21, 2q21, 8p23, 8q24, 9q22, 14q31, and 19p13 (Bignell, Canzian et al. 1997, Canzian, Amati et al. 1998, Malchoff, Sarfarazi et al. 2000, Cavaco, Batista et al. 2008, He, Nagy et al. 2009, Tomaz, Sousa et al. 2012). Definitive germline genetic mutations underlying thyroid cancer predisposition remain yet to be identified within candidate genes in these regions. Thyroid tumor development likely involves a complex interplay between genetic predisposition and environmental risk factors (Hsiao and Nikiforov 2014).

The incidence of thyroid cancer is about three to four times higher among females than males worldwide, ranking the sixth most common malignancy diagnosed in women. By 2019, one study predicts that PTC will become the third most common cancer in women at a cost of \$19–21 billion in the United States. Optimization of long term health outcomes and education about potential prognosis for individuals with thyroid neoplasms is critically important.

Among women, papillary thyroid cancer incidence rates are higher among Asians (10.96 per 100 000 woman-years) and lower among blacks (4.9 per 100 000 woman-years). Among men, papillary thyroid cancer incidence rates are higher



among whites (3.58 per 100 000 woman-years) and lower among blacks (1.56 per 100 000 woman-years) (Aschebrook-Kilfoy, Grogan et al. 2013).

The incidence of follicular thyroid cancer in the USA is 0.82 per 100 000 person-years, with rates of 1.06 per 100 000 woman-years and 0.59 per 100 000 man-years.

The incidence of follicular cancer does not vary substantially by race/ethnicity. The incidence rates of medullary thyroid cancer (MTC) and anaplastic thyroid cancer (ATC) are 0.11 and 0.21 per 100 000 person years with no noted substantial differences by race/ethnicity and sex, respectively (Aschebrook-Kilfoy, Grogan et al. 2013).

Thyroid cancer can occur at any age but it is rare in childhood. Most tumors are diagnosed during third to sixth decade of life. The age-adjusted death rate was 0.5 per 100 000 men and women per year, increasing from 0.1% under age 20%–30% in the seventh and the eighth decades.

Despite increasing incidence, the mortality from thyroid cancer has tended to decline over the last three decades. It is unclear how much of the decline in mortality is due to better diagnosis rather than to improved treatment of thyroid neoplasm.

The 5-year relative survival rates reported for patients with papillary and follicular carcinomas (stages I-II) are 98% and 90% respectively (Hundahl, Fleming et al. 1998).

1.1.3 Diagnostic Criteria

Thyroid cancer presents as a thyroid nodule detected by palpation and more often by neck US. Thyroid nodules are a common clinical problem. While thyroid



nodules are common (4%–50% depending on the diagnostic procedures and patients' age)(Dean and Gharib 2008), thyroid cancer is rare (~5% of all thyroid nodules). Epidemiologic studies have shown the prevalence of palpable thyroid nodules to be approximately 5% in women and 1% in men living in iodine-sufficient parts of the world (Tunbridge, Evered et al. 1977). Epidemiologic studies have shown the prevalence of palpable thyroid nodules to be approximately 5% in women and 1% in men living in iodine-sufficient parts of the world (Vander, Gaston et al. 1968, Tunbridge, Evered et al. 1977).

Thyroid high-resolution ultrasound (US) is a widespread technique that is used as a first-line diagnostic procedure for detecting and characterizing nodular thyroid disease (I, A). The US can detect thyroid nodules in 19%–68% of randomly selected individuals, with higher frequencies in women and the elderly (Tan and Gharib 1997, Guth, Theune et al. 2009).

The clinical importance of thyroid nodules rests with the need to exclude thyroid cancer, which occurs in 7%–15% of cases depending on age, sex, radiation exposure history, family history, and other factors (Hegedus 2004, Mandel 2004).

According to last guidelines published by ATA in 2016 a diagnostic thyroid/neck US should be performed in all patients with a suspected thyroid nodule, nodular goiter, or radiographic abnormality suggesting a thyroid nodule incidentally detected on another imaging study (Haugen, Alexander et al. 2016).

US features associated with malignancy are hypoechogenicity, microcalcifications, absence of peripheral halo, irregular borders, solid aspect, intranodular blood flow and shape (taller than wide). Each of these patterns taken individually is poorly



predictive. When multiple patterns suggestive of malignancy are simultaneously present in a nodule, the specificity of US increases but the sensitivity becomes unacceptably low (Pacini, Schlumberger et al. 2006).

The pattern of sonographic features associated with a nodule confers a risk of malignancy, and combined with nodule size, guides FNA decision-making (see Recommendation 8 of ATA guidelines)(Smith-Bindman, Lebda et al. 2013, Brito, Gionfriddo et al. 2014).

Fine needle aspiration cytology (FNAC) is an important technique that is used along with US for the diagnosis of thyroid nodules. FNA is the procedure of choice in the evaluation of thyroid nodules, when clinically indicated. FNAC should be performed in any thyroid nodule >1 cm and in those <1 cm if there is any clinical (history of head and neck irradiation, family history of thyroid cancer, suspicious features at palpation, presence of cervical adenopathy) or ultrasonographic suspicion of malignancy. In the case of multinodular goiter, those with suspicious features at US should be submitted to FNAC. FNAC is a very sensitive tool for the differential diagnosis of benign and malignant nodules although there are limitations: inadequate samples and follicular neoplasia. In the event of inadequate samples, FNAC should be repeated, while in the case of follicular neoplasia, with normal thyroid stimulating hormone (TSH) and 'cold' appearance at thyroid scan, surgery should be considered (Pacini, Schlumberger et al. 2006).

The use of various immunohistochemical markers in cytologic samples to differentiate papillary thyroid carcinoma from other follicular derived lesions of thyroid has been explored during the last years but none of the markers appears to



be specific enough to be employed as the diagnostic marker for the cytologic diagnosis of papillary thyroid carcinoma. Recently, it has been reported that by molecular testing for thyroid nodules (BRAF, RAS, RET/PTC and PAX8/PPAR γ mutations), the presence of any mutation was a strong indicator of cancer because ~97% of mutation-positive nodules had malignant diagnosis at histology.^{1,2} Thyroid function test and thyroglobulin (Tg) measurement are of little help in the diagnosis of thyroid cancer. However, measurement of serum calcitonin (CT) is a reliable tool for the diagnosis of the few cases of MTC (5%–7% of all thyroid cancers) and has higher sensitivity compared with FNAC. For this reason, measurement of CT should be an integral part of the diagnostic evaluation of thyroid nodules (Pacini, Schlumberger et al. 2006).

1.1.4 Molecular testing in thyroid cancer

Thyroid molecular testing initially was developed to reduce unnecessary diagnostic thyroid surgery for indeterminate thyroid nodules. The initial development of immunohistochemical evaluation with Galectin-3 and other biomarkers demonstrated some potential to improve the diagnostic accuracy of thyroid cytology, but it lacked sufficient reproducibility and sensitivity to reliably exclude malignancy (Bartolazzi, Orlandi et al. 2008). Subsequently, new investigations sought to identify specific gene mutations and gene rearrangements that were pathogenic in thyroid cancer. The feasibility of cytomolecular testing for known DNA and RNA mutations, which accounted for 70% of thyroid carcinomas (Harvey rat sarcoma viral oncogene homolog [H-Ras], neuroblastoma rat sarcoma viral



oncogene homolog [N-Ras], Kirsten rat sarcoma viral oncogene homolog [K-Ras], rearranged during transfection/PTC 1 [Ret/PTC1], Ret/PTC2, Ret/PTC3, v-Raf murine sarcoma viral oncogene homolog B1 [BRAF], and paired box gene 8-peroxisome proliferator-activator receptor γ [Pax8-PPAR γ]) was demonstrated, which improved the diagnostic accuracy of needle biopsy when added to cytologic evaluation (Fig.5). The most common mutations identified in thyroid cancer improved the specificity of thyroid cytology, but it was still not a sensitive enough detection method to rule out cancer for cases in which no mutation was identified (Nikiforov, Steward et al. 2009).



Mitogen Activated Protein Kinase (MAPK) Cascade

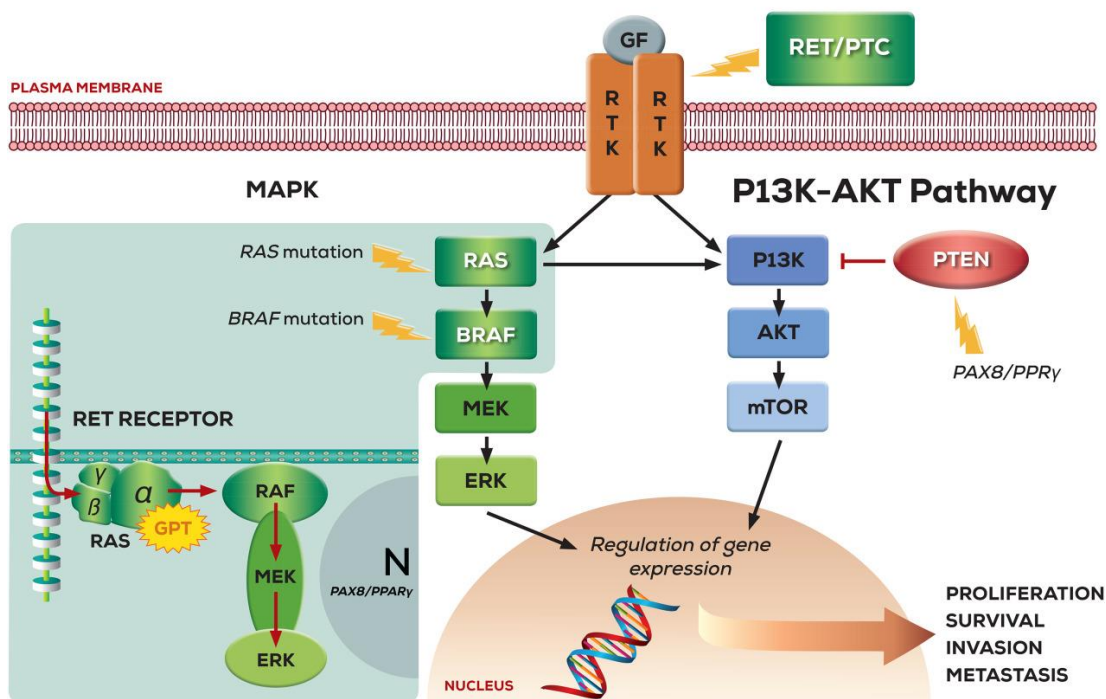


Fig. 5 The mitogen-activated protein kinase pathway is the principal pathway leading to differentiated thyroid cancer. The PI3K-AKT pathway is an important pathway leading to follicular thyroid cancer and undifferentiated thyroid cancer. α , β , and γ indicate rearranged during transfection (RET) receptors α , β , and γ , respectively; BRAF, v-Raf murine sarcoma viral oncogene homolog B1; ERK, extracellular signal-regulated kinase; GF, growth factor; GPT, glutamic-pyruvic transaminase; H-Ras, Harvey rat sarcoma viral oncogene homolog; K-Ras, Kirsten rat sarcoma viral oncogene homolog; MEK, mitogen activated protein extracellular signal-regulated kinase; mTOR, mammalian target of rapamycin; N, nucleus; N-Ras, neuroblastoma rat sarcoma viral oncogene homolog; Pax8/PPAR γ , paired box gene 8-peroxisome proliferator-activator receptor γ ; PTEN, phosphatase and tensin homolog; RAF, RAF proto-oncogene serine/threonine-protein kinase; RAS, a family of rat sarcoma (ras) small guanosine triphosphate hydrolases (GTPases); RET, rearranged during transfection; Ret/PTC, rearranged during transfection/papillary thyroid cancer 1; RTK, receptor tyrosine kinase. (Roth, Witt et al. 2018)

In addition, as molecular testing was beginning to develop for clinical use to improve the diagnostic accuracy of thyroid FNA, The Cancer Genome Atlas (TCGA) project mapped the mutations attributed to both classical and follicular variants of PTC, significantly reducing the number of unknown specific mutations causing differentiated thyroid cancer. Incorporating the new information obtained through TCGA, an updated gene panel using next-generation sequencing (NGS) was developed for clinical use (ThyroSeq NGS, v2.0 [and now v2.1]; CBLPath, Orlando, Fla) (Nikiforova, Wald et al. 2013, Nikiforov, Carty et al. 2014). This test was developed to improve the overall accuracy of molecular testing to identify both benign and malignant thyroid cytopathology by improving sensitivity and negative predictive value (NPV) with only a mild reduction in specificity and positive predictive value (PPV).

“Ruling Out”

A primary goal of molecular testing of indeterminate FNA samples is to identify patients who can avoid unnecessary surgery – while minimizing the risk of missing cancer. This requires a test to have a high sensitivity and, correspondingly, a high NPV. Up until a few years ago, such use of molecular testing was primarily limited to academic settings and early tests showed lower-than-desired sensitivity rates (Mazzanti, Zeiger et al. 2004, Lubitz, Ugras et al. 2006, Prasad, Somervell et al. 2008).

In 2011, the commercial introduction of a 167-gene classifier (Afirma® Gene Expression Classifier, or GEC) that identified benign nodules among those deemed



indeterminate by cytopathology changed the trajectory for how molecular testing is used in thyroid cancer diagnosis.

The 167-gene classifier is performed on patient samples that are collected during the initial FNA procedure, removing the need for patients to undergo a follow-up FNA procedure. The test uses mRNA expression data obtained through microarray analysis and machine learning to identify benign nodules among those previously classified as indeterminate. In a blinded, prospective clinical validation study of the locked gene classifier in 49 sites, Alexander et al. (Alexander, Kennedy et al. 2012) determined that the classifier had a sensitivity of 92% and an NPV of 94% and 95% for AUS/FLUS and FN/SFN, respectively, among patients with a pretest malignancy rate of 32%. These rates are similar in accuracy to those of a benign cytopathology result.

Clinical utility data demonstrated that use of the 167-gene classifier changed patient care as intended. In a multicenter study, Duick et al (Duick, Klopper et al. 2012) showed that surgeries among patients with “benign” GEC results were reduced by 90% (from 74% to 7.6%), compared to historical surgery rates for patients with indeterminate nodules. Additional studies demonstrated the durability of a benign GEC result, as patients were followed clinically over an extended period of time and remained cancer free.

Subsequent classifiers have been introduced, which also combine genomic data and machine learning to identify benign nodules. One test (RosettaGx Reveal) is performed on a slide smear from the initial FNA biopsy in order to avoid the need for a separate collection tube and FNA pass. In a clinical validation study, Lithwick-



Yanai et al (Lithwick-Yanai, Dromi et al. 2017) reported that the test had a sensitivity of 74% for Bethesda III and IV nodules.

“Ruling In”

Gene mutation testing requires examining specific genes for alterations associated with cancer. It often includes testing BRAF, and three RAS genes for specific point mutations and testing for three gene fusions: RET/PTC 1, RET/PTC3, and PAX8/PPARG. This type of molecular testing has been considered primarily as a “rule in” test for cancer due to its typically higher specificity for cancer, yet lower sensitivity. In thyroid nodules with indeterminate cytology, the sensitivity of this seven-gene mutational panel test is variable, with reports ranging from 36% to 100% (Nikiforov, Steward et al. 2009, Nikiforov, Ohori et al. 2011, Beaudenon-Huibregtse, Alexander et al. 2014, Eszlinger, Bohme et al. 2017).

According to the 2015 ATA guidelines (Haugen, Alexander et al. 2016), the reported variability in sensitivity of mutational analysis with the seven-gene panel in indeterminate nodules suggests that mutation panels of this size may not reliably rule out malignancy with a negative test in this population. At the same time, molecular testing should only be used if the results will change the surgical decision-making (Haugen, Alexander et al. 2016).


Since most patients with indeterminate thyroid nodules are already directed to surgery, use of a mutation panel that rules in cancer would only change management in the few patients that are initially being considered for observation, or if the extent



of surgery were altered due to the risk of cancer associated with the specific genomic alteration.

A subsequent version of the mutation panel test (ThyroSeq® 2.1) includes 56 genes and promises a high accuracy in identifying both cancerous and benign nodules, which enables it to rule in and rule out cancer (Nikiforov, Carty et al. 2014, Nikiforov, Carty et al. 2015). These findings were based on single-center studies in which the treating physician and histopathologist were unblinded to some of the molecular results. An evaluation by Valderrabano et al concluded that more study was needed after their analysis demonstrated significantly lower sensitivity and specificity for the test compared to the initial validation findings. For example, in their evaluation, the test's sensitivity was 70%, meaning that it missed 30% of the cancers in the study group (Valderrabano, Khazai et al. 2017).

The notion that mutation does not equal malignancy, and vice versa, was demonstrated by Pagan et al (Pagan, Kloos et al. 2016). In this study, a 524-gene panel encompassing 851 variants and 133 fusions known to be associated with thyroid cancer was used to evaluate thyroid nodule samples. The researchers found that gene alterations appeared in only 50% of the cancerous samples (ie, 50% sensitivity) and 20% of the benign thyroid samples harbored gene alterations (ie, 80% specificity). These findings suggest that the test lacked accuracy in ruling cancer in or out because gene mutations were found in both benign and malignant samples and similarly were not present in both types of samples (Pagan, Kloos et al. 2016).



1.2 Raman spectroscopy

Advanced in cancer diagnostic play a pivotal role in increasing early detection of cancer and improving the chances of successful treatment. Up to date, diagnostic pathways are complex and may involve many diagnostic tests such as X-ray, computed tomography, ultra-sound, and endoscopy, but currently histopathology remains the “gold standard” investigation. However, this method is invasive, requiring removal of tissue, often randomly and unnecessarily. Tissue fixation, sectioning and staining follow which can be costly and slow. Histological analysis is very subjective and is associated with considerable inter-observer disagreement (Montgomery, Bronner et al. 2001).

Other diagnostic and screening methods may involve the use of ionising radiation as a precursor to histopathology, for example in breast cancer screening women undergo mammography to identify micro-calcification. Diagnostic methods, which could potentially avoid the use of ionising radiation, would have significant benefits. A minimally invasive, accurate, reproducible, rapid, non-destructive and cost effective tool is required.

In this setting, Raman spectroscopy (RS) is one of the promising techniques that may increase the reliability and decrease the diagnosis time by providing very specific molecular information from a tissue or a sensing system. Cells and tissues are characterized by a specific biochemical composition and molecular structure. In a similar way, each pathology or cellular abnormality is accompanied by biochemical and molecular changes. Optical and spectroscopic techniques that



correlate the biochemical composition, molecular structure, and their variations with the diagnosis would provide powerful clinical tools.

Due to the fact that RS can provide molecular level information about the composition of a sample, the gradual biochemical changes from a healthy tissue to a tumor is reflected in a Raman spectrum. The observed spectral differences are attributed to the changes in the biomacromolecular composition of the tissues as it progresses to form tumor.

For these reasons, RS is beginning to gain recognition as a potential adjunct to histopathology due to the fact the method can overcome the limitations of current diagnostic techniques. Recent advances in RS have promoted it to a level at which in vivo trials are beginning to emerge. When used in combination with powerful multivariate algorithms the technique can potentially provide automated, objective and reproducible classification of pathology in clinically relevant time frames (Kallaway, Almond et al. 2013).

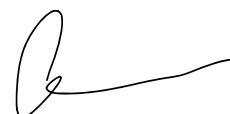
1.2.1 Raman spectroscopy technique

Raman spectroscopy is a vibrational spectroscopic technique and it provides chemical information from a molecule or molecular structure. RS enables the elucidation of a tissue's biochemical fingerprint by measuring the molecular specific inelastic scattering of light. The physical mechanism behind Raman spectroscopy is inelastic light scattering of monochromatic laser radiation, which was experimentally discovered in the late 1920^s.



All biomolecules, including proteins, lipids, nucleic acids, carbohydrates, and metabolites, are simultaneously probed within complex matrices without preparation, even under in-vivo conditions.

Primarily, RS requires the illumination of a tissue sample with a monochromatic laser and subsequent collection and analysis of the scattered light for intensity and wavelength. Photons in the incident laser light undergo inelastic collisions with molecules, causing an exchange of energy and therefore a change in frequency. The frequency change, known as the Raman shift, is specific to the species of molecule causing the scattering and can be defined as the difference between incoming and scattered photons. Larger shifts indicate that more energy is required to bring about a particular vibrational motion. The shift is independent of the wavelength of excitation, which means that the energy shift is constant for each separate molecular species. The intensity of the peak is directly proportional to the relative concentration of the sum of molecular constituents giving rise to that peak. Thus, the Raman spectrum is a direct function of the molecular composition of the interrogated volume within the tissue, giving us a complex molecular fingerprint. Since the Raman spectrum of a molecule is a 'fingerprint' and the bands on a spectrum have a narrow bandwidth, a Raman spectrum from a molecular mixture can provide molecular level information about its chemical composition. As example, Figure 6 reports a Raman spectrum of esophageal tissue measured using 830 nm excitation.



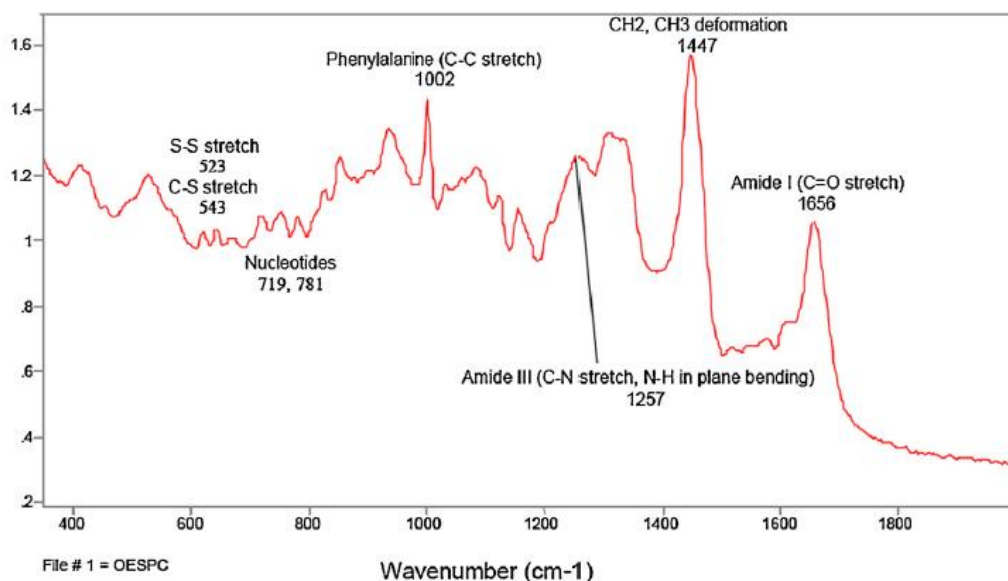


Fig. 6: Raman spectrum of esophageal tissue measured using 830 nm excitation. Characteristic biochemical peaks have been labelled. Variations in peak height and position can be detected in tissue spectra and have been shown to indicate biochemical progression towards malignancy (Upchurch, Isabelle et al. 2018).

Fortunately, the majority of biological molecules are Raman active, each with their own fingerprint. As a result, RS is highly sensitive to subtle biochemical and molecular changes, which is vital in the differentiation of tissue samples. This property makes it potentially a very powerful diagnostic tool. As example of its high sensitivity, Figure 7 shows Raman spectral biochemical signatures of differing pathologies within a single esophageal biopsy.

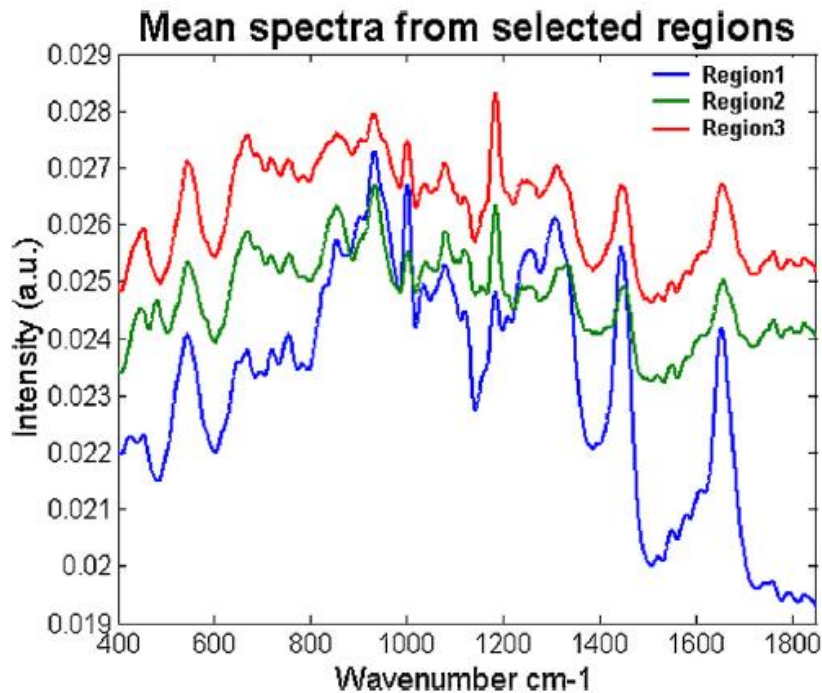


Fig. 7: Raman spectral biochemical signatures of differing pathologies within a single esophageal biopsy. Indicating the amount of information that can be obtained with Raman spectroscopy (Upchurch, Isabelle et al. 2018).

However, its inherently low scattering efficiency has hampered the use of RS until the development of powerful lasers and sensitive detectors. Over the past decade, progress in Raman spectroscopic instrumentation has increased in the sensitivity of its measurement capability to such an extent that the acquisition of high quality spectral data from biological tissue and samples is possible.

1.2.2 The role of Raman spectroscopy for cancer diagnosis

Almost all of the cancer diagnosis applications of technique focus on tissue examinations either *in vivo* or *ex vivo* by detecting a biomarker in a body fluid.

Up to date, the main developments are noted to be:

- **In vivo applications**

In vivo, RS offers the potential for “optical biopsy” with important clinical benefits. For in vivo applications, it is ideal to use a fiber optic probe to guide the laser light to the target and collect Raman scattering. It can also be embedded into an endoscopy device.

Excisional tissue endoscopic biopsy carries risks of bleeding and visceral perforation, as well as removal of normal tissue unnecessarily. RS would obviate the need for this, thus reducing trauma to the patient, reducing clinician workload, and reducing secondary repeat procedures.

It will also decrease the rate of re-excisions of areas of dysplasia or malignancy by accurately defining resection margins (Hanlon, Manoharan et al. 2000). Raman spectroscopy (RS) is suitable for use with fiber-optic probes making it potentially ideal as a medical diagnostic tool for assessment of hollow organs such as esophagus (Kendall, Stone et al. 2003), bladder (Crow, Molckovsky et al. 2005) and larynx (Stone, Stavroulaki et al. 2000).

One of the major fields of application of RS in endoscopy is the identification of Barrett's esophagus. Barrett's esophagus is a complication of chronic gastroesophageal reflux and considered as the predisposition for dysplasia. Therefore, its early detection may provide an opportunity for the prevention of cancer formation. The endoscopic examination of the suspicious regions is the current approach for the identification of these lesions. However, it is extremely difficult to identify these lesions with a white light endoscopy procedure. Therefore,



the development of a fiber-optic based Raman probe is very important to increase the diagnosis accuracy of Barrett's esophagus. Recently, Bergholt et al. report the use of a fiber-optic embedded into an endoscopy device was used to collect Raman scattering with the guidance of wide field endoscopic, narrow-band and auto-fluorescence imaging. The Raman spectra from a total of 75 sites (42 healthy and 33 tumor sites) from 27 patients were acquired during the endoscopic examination. The study concluded that RS could provide valuable in vivo biochemical information for diagnosis (Bergholt, Zheng et al. 2013). Figure 8 reports a schematic diagram of the rapid multiplexing Raman spectroscopy technique during endoscopy.

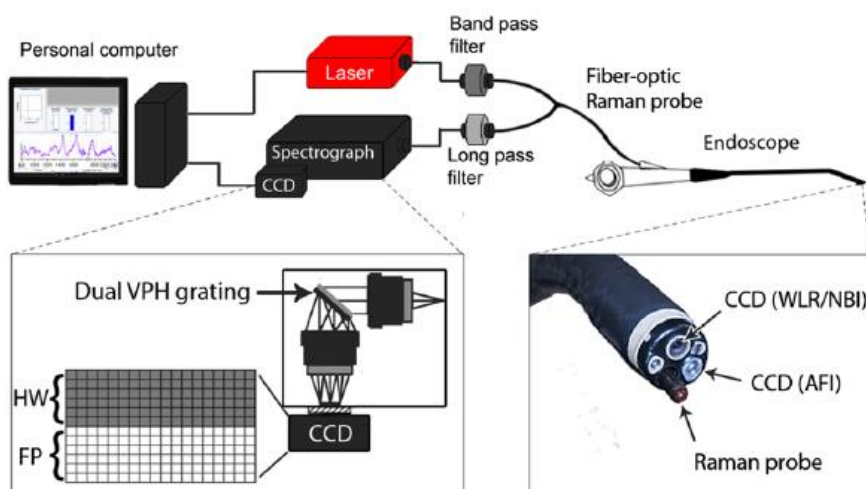


Fig. 8: Schematic diagram of the rapid multiplexing Raman spectroscopy technique for simultaneous acquisition of both the fingerprint (FP) and high wavenumber (HW) Raman spectra under trimodal endoscopic imaging [i.e., white light reflectance (WLR), narrowband imaging (NBI), autofluorescence imaging (AFI)] guidance. A customized dual-transmission VPH grating is incorporated into the Raman system for dispersion of FP and HW Raman spectra onto different vertical segments of a CCD (Bergholt, Zheng et al. 2013).

Furthermore, in vivo applications can provide real time and label-free biochemical information about the status of a lesion, which can be used to make diagnostic decision or to find the borders of a tumor during surgery (Karabeber, Huang et al. 2014, Kong, Zaabar et al. 2014). 'Optical biopsy' can be a very vital tool during surgery to completely remove cancerous tissue during neurosurgery to prevent its recurrence as reported by Jermyn et al (Jermyn, Mok et al. 2015). This can be extremely useful since the identification of the borders of a cancerous growth is very difficult with current imaging techniques. Figure 9 shows an example of handheld contact fiber-optic probe for Raman spectroscopy used during neurosurgery.

A handwritten signature in black ink, consisting of a stylized initial 'B' followed by a horizontal line extending to the right.

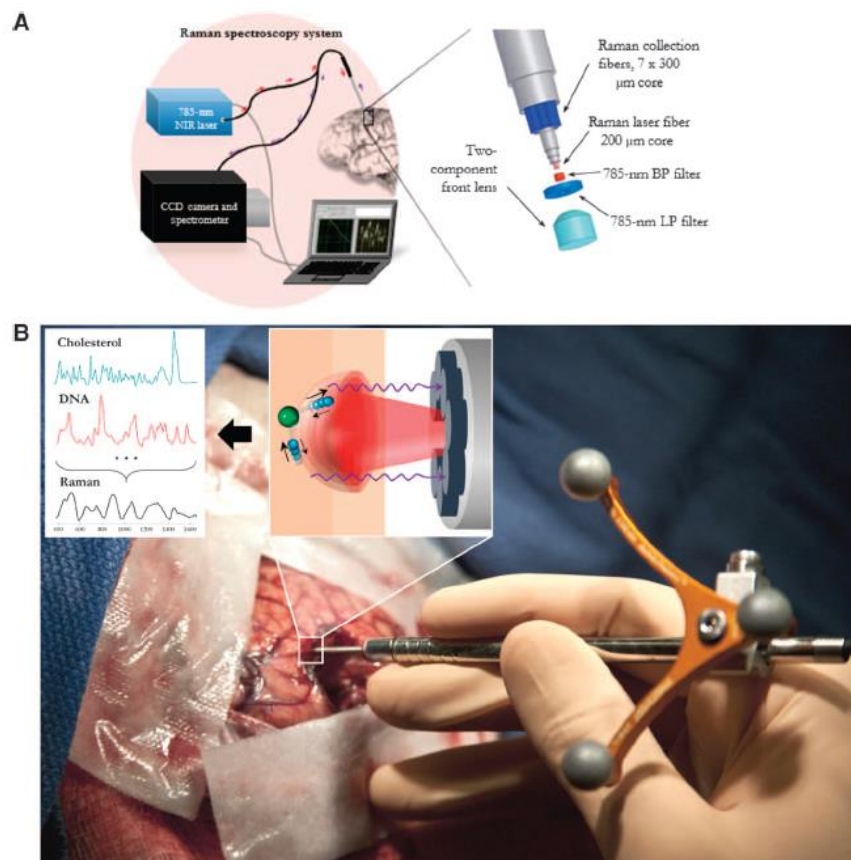


Fig. 9: (A) Experimental setup diagram with the 785-nm NIR laser and the high-resolution CCD spectroscopic detector used with the Raman fiber optic probe. (B) The probe (Emvision, LLC) was used by authors to interrogate brain tissue during surgery (Jermyn, Mok et al. 2015).

- **Histopathology tools**

In ex vivo applications, the tissue samples are either used directly or sliced to acquire Raman spectra in a similar way as tissue slices prepared for histopathological examination.

The majority of ex vivo studies has been performed on tissue sections. In large there has been a trend towards imaging/mapping approaches and so called ‘histopathology tools’ because they mimic the morphological appearance of current

histopathology methods but include additional biochemically specific information.

Raman spectroscopy has demonstrated its potential in aiding pathologists in the identification and objective classification of subtle biochemical changes related to carcinogenesis. There are several studies demonstrating the feasibility of the technique for the analysis of excised tissues directly without any preparation or sliced tissue sections (Barroso, Smits et al. 2015).

Recently, for example, Bergner (Bergner, Romeike et al. 2013) reports the possibility of discrimination between oral cancer and healthy tissue based on water content determined by Raman Spectroscopy (Figure 10).

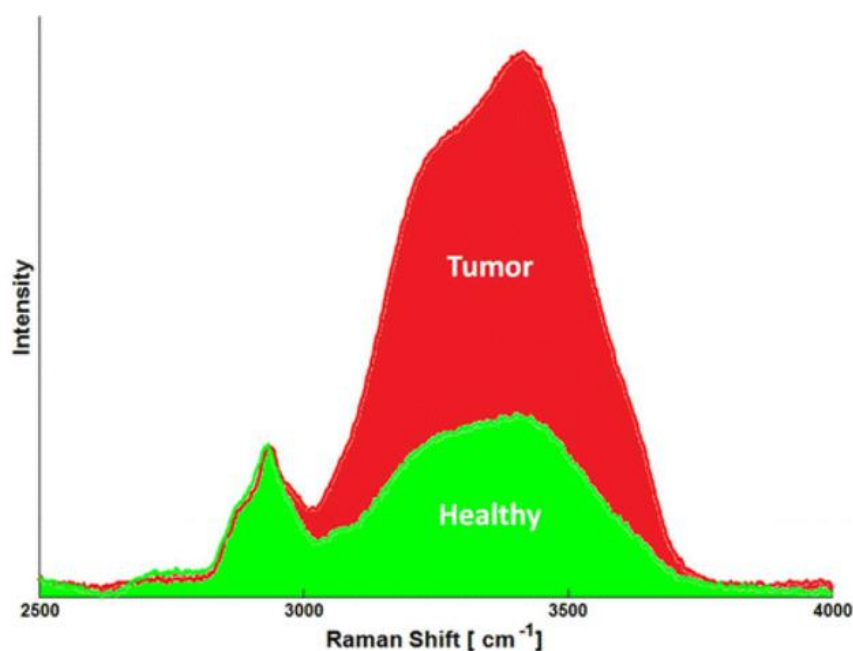


Fig. 10: Discrimination between oral cancer and healthy tissue based on water content determined by Raman Spectroscopy (Bergner, Romeike et al. 2013).

Tumor-positive resection margins are a major problem in oral cancer surgery. The authors investigate the use of Raman spectroscopy to differentiate tumor from surrounding healthy tissue in oral squamous cell carcinoma. From 14 patients undergoing tongue resection for squamous cell carcinoma, the water content was determined at 170 locations on freshly excised tongue specimens using the Raman bands of the OH-stretching vibrations (3350–3550 cm^{-1}) and of the CH-stretching vibrations (2910–2965 cm^{-1}). The results were correlated with histopathological assessment of hematoxylin and eosin stained thin tissue sections obtained from the Raman measurement locations. The water content values from squamous cell carcinoma measurements were significantly higher than from surrounding healthy tissue (p -value < 0.0001). Tumor tissue could be detected with a sensitivity of 99% and a specificity of 92% using a cut-off water content value of 69%. Because the Raman measurements are fast and can be carried out on freshly excised tissue without any tissue preparation, this finding signifies an important step toward the development of an intraoperative tool for tumor resection guidance with the aim of enabling oncological radical surgery and improvement of patient outcome.

- **Deep Raman tools for in vivo analysis in solid organs**

‘Deep Raman spectroscopy’ is another application that is being developed for non-invasive diagnosis of solid organs that can be achieved from outside of the body. At this stage of development it can only be applied to specific applications where the Raman signature is very strong and distinct as there is a trade off with the intensity of the signature obtained from depth. This application has been tested in



the study of calcification associated with breast cancer (Baker, Matousek et al. 2007, Stone, Baker et al. 2007, Stone and Matousek 2008). The above mentioned studies report the possibility of utilizing Spatially offset Raman spectroscopy (SORS) for measuring calcification composition through varying thicknesses of tissues (2 to 10 mm), which is about one to two orders of magnitude deeper than has been possible with conventional Raman approaches (Figure 11). This result secures the first step in taking this technique forward for clinical applications seeking to use Raman spectroscopy as an adjunct to mammography for early diagnosis of breast cancer, by utilizing both soft tissue and calcification signals. Non-invasive elucidation of calcification composition, and hence type, associated with benign or malignant lesions, could eliminate the requirement for biopsy in many patients.

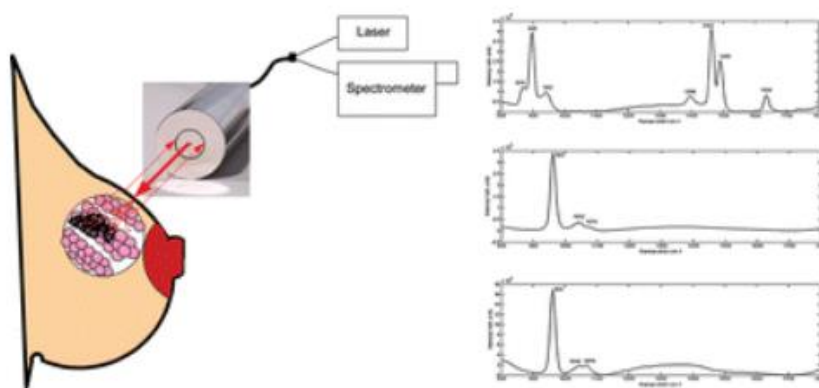


Fig. 11: Here is reported the first demonstration of SORS for potential in vivo breast analysis (Baker, Matousek et al. 2007).

- **Detection of cancer biomarkers**

The detection of cancer marker in body fluids for clinical decision-making is an exciting approach, which may allow screening to detect cancer formation as early as possible and simplify the early diagnosis process. An increased concentration of cancer markers can be detected in urine, saliva and blood. In a study, the detection of tumor suppressor p53 and cyclin-dependent kinase inhibitor p21 was demonstrated with a Surface-Enhanced Raman Scattering (SERS) -based immunoassay. The p53 and p21 quantifications in blood serum were performed from the two different Raman reporters (4MBA and DTNB). The authors claim excellent specificity, high sensitivity and very high reproducibility of the assay (Wu, Wang et al. 2013).

Another way that the technique can be utilized is the detection of cancer markers. A SERS based method for the quantitative determination of haptoglobin, a plasma glycoprotein and a prognostic ovarian cancer biomarker, was reported (Perumal, Balasundaram et al. 2015).

Several authors suggested that, increased adenosine concentration, usually related with tumor formation, can be used as biomarkers for cancer formation (Zhang, Wang et al. 2010).

Finally, RS can provide rapid, reproducible, non-destructive measurement of disease specific tissue composition, which when combined with powerful mathematical algorithms allow objective classification. Numerous spectral classification models are under development for both optical biopsy (probe) applications³ and histology tool (mapping) applications. Initially, early studies




focused on differentiating normal tissue and advanced cancers. However, with developing technology and complex analytical methods, there has been a move towards diagnosis of neoplastic change at much earlier stages.

1.2.3 Raman spectroscopy in thyroid cancer

Up to date only two studies have investigated the role of Raman spectroscopy in thyroid cancer. The first one, performed by Harris et al.(Harris, Garg et al. 2009), aimed to investigate whether RS combined with advanced mathematical modeling (neural networks) could discriminate between 2 commercial thyroid cell lines; an human thyroid anaplastic carcinoma cell line (8305C) and a “normal” commercial cell line (Nthy-ori 3-1) obtained from the European Collection of Cell cultures (ECACC). Raman spectra were obtained using a Renishaw 'System 1000' Raman microscope while excitation was provided by a Sacher Lasertechnik Littrow external cavity laser set at 783 nm. Finally, detection of the Raman scattered light was performed with a Renishaw RenCam NIR enhanced CCD camera.

The authors obtained 52 spectra from the Nthy-ori 3-1 cells and 64 spectra from the 8305C cells.

Figure 12 and 13 report the typical Raman spectrum from the non-cancerous and cancerous thyroid cell lines.



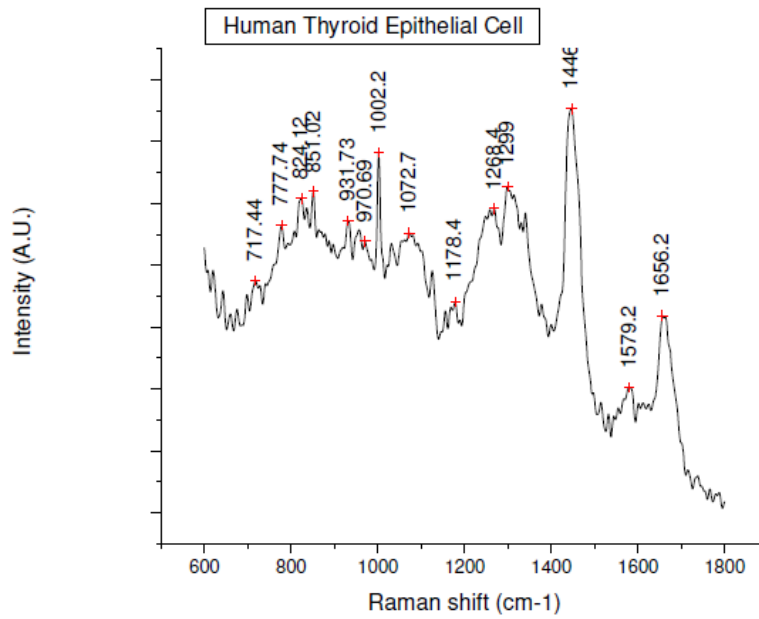


Fig. 12: Typical Raman spectrum from the Human thyroid epithelial cell (Nthy-ori 3-1); a non-cancerous cell line (Harris, Garg et al. 2009).

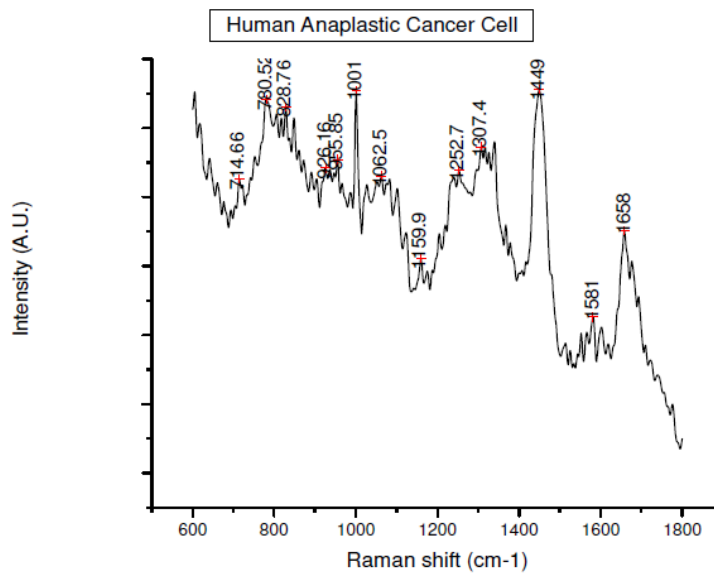


Fig. 13: Typical Raman spectrum from a Human anaplastic thyroid cancer cell (8305C); a cancerous cell line (Harris, Garg et al. 2009).

In the study, the authors also report The PCA (Principal Component analysis) plot of non-cancerous and cancerous thyroid cell lines. This plot, reported in figure 14, is not totally discriminatory even if it show a distinct clustering of normal and cancerous cell lines but the overlap is too great to be diagnostic.

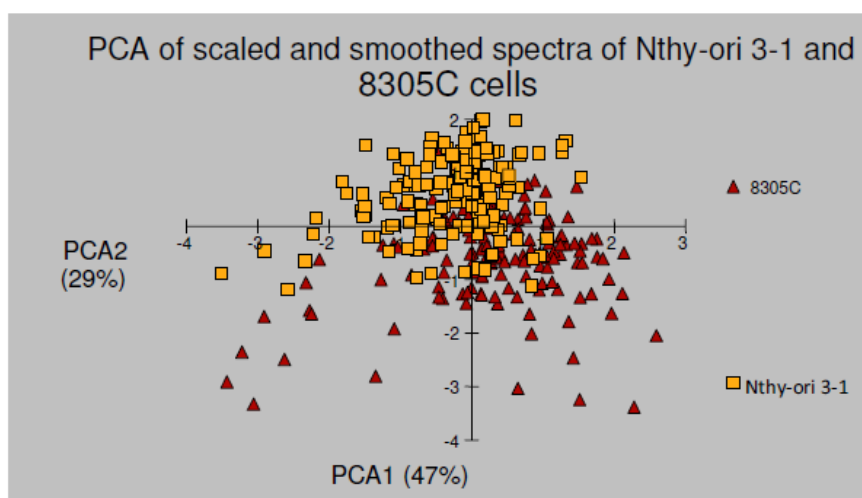


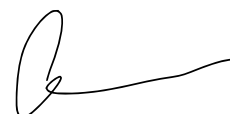
Fig. 14: The results of PCA comparing the non-cancerous (Nthy-ori 3-1) and cancerous (8305C) cell lines from the Raman spectra results (Harris, Garg et al. 2009).

However the neural network result for the Raman data, provide a 95% sensitivity for the cancerous cell line and 92% sensitivity for normal cell line demonstrating that Raman spectroscopy, coupled with neural network analysis is able to

discriminate between cancer and non-cancer cells in a simple model system with a high degree of accuracy.

Teixeira et al. report a thyroid tissue analysis through Raman spectroscopy in 2009 (Teixeira, Bitar et al. 2009). The objective of the above-mentioned work was to study the biochemical alterations of tissues of the thyroid gland by means of molecular vibrations probed by FT-Raman spectroscopy. After the surgical procedure (Thyroidectomy), 27 fragments of the thyroid were collected from 18 patients, comprising the following histologic group: goiter adjacent tissue, goiter nodular region, follicular adenoma, follicular carcinoma and papillary carcinoma. The authors, through the discriminative linear analysis of the Raman spectra of the tissue, established (in percentages) the correct classification index among the groups.

For the group's goiter adjacent tissue versus goiter nodular region, a result of 58.3% of correct classification was obtained; this percentage was low, and it was not possible to discriminate the FT-Raman spectra of these two groups. Figure 15 shows the median between the spectra of the goiter adjacent tissue (black line) and the nodular region goiter (grey line). These spectral modifications were not significant enough to represent a relevant separation between them. The reported data justify the statement of Layfield et al. (Layfield, Wax et al. 2003) that adenomatous goiter is a hyperplasia, with no considerable cellular alterations; this also justifies the similarity between normal thyroid and adenomatous goiter, or adjacent and central tissues of a goiter injury.



Interestingly the authors analyzed the difference between adenomatous goiter, follicular adenoma and follicular carcinoma. The relative median spectra were analyzed and reported in figure 16.

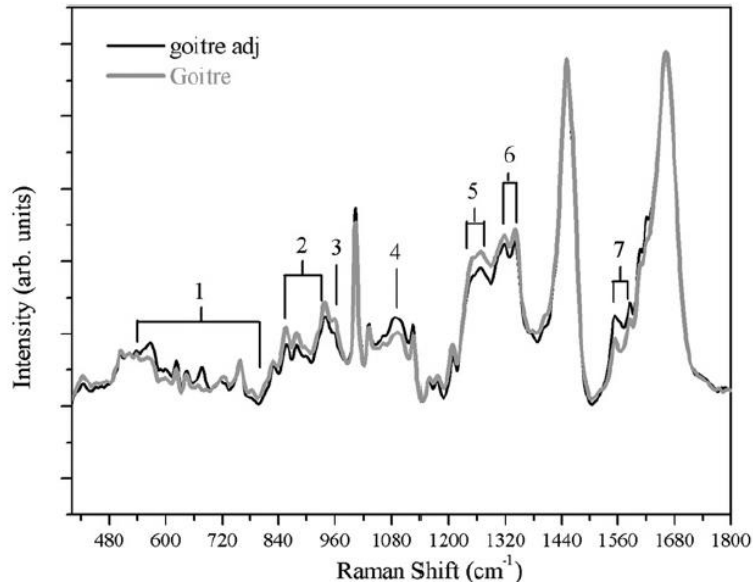


Fig. 15: The median between the spectra of goiter adjacent tissue (black line) and the nodular region goiter (grey line) (Layfield, Wax et al. 2003).

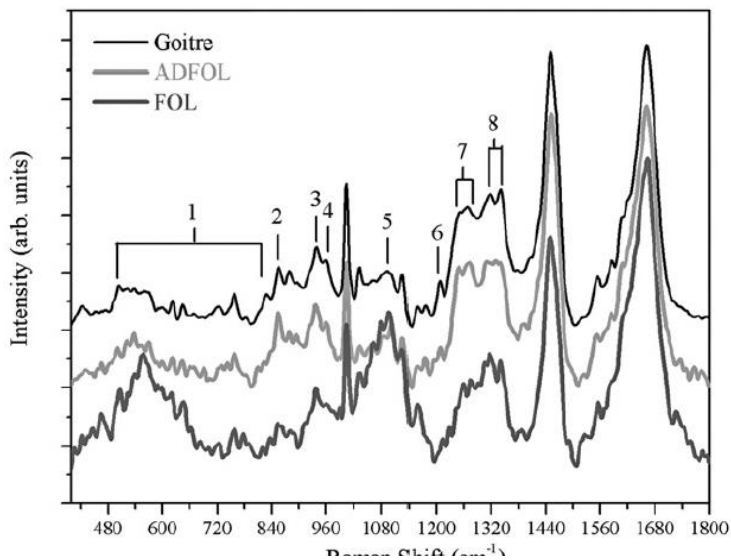
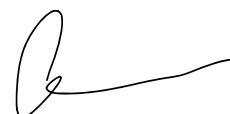


Fig. 16: Median of the adenomatous goiter spectra (black line), follicular adenoma (grey line) and follicular carcinoma (dark grey line) (Layfield, Wax et al. 2003).

From this figure, it can be noted that some peaks appear in all three spectra; that is, the biochemical compositions are nearly the same in all three-tissue types, although with different intensities among them. According the authors, these regions could be similar to those considered characteristic of the normal thyroidal tissue. However, there are also characteristic peaks for only one or two types of injuries, those being the modes of more relevance to differentiate the pathologies for they are exclusive and representative peaks of tissue alteration. Interestingly the authors invite to draw attention to the 1095 cm^{-1} band, which is characteristic of the follicular carcinoma and follicular adenoma tissues since it did not appear on the goiter nodular region. The follicular adenoma, on the other hand, has peaks with high intensity at 856, 937, and 960 cm^{-1} . The characteristic peaks for follicular carcinoma are from 500 to 840, 1095, 1258–1290, and 1315–1339 cm^{-1} .

Finally, the correct classification index reported between goiter (nodular region and periphery) and papillary carcinoma was 64.9%. However, relevant results were obtained in the analysis of the spectra in the benign tissues (goiter and follicular adenoma) versus malignant tissues (papillary and follicular carcinomas) analysis, for which the percentage was 72.5%, which was considered very well. The median of the adenomatous goiter spectra (black line), papillary carcinoma (grey line) and follicular carcinoma (dark grey line) is reported in Figure 17.



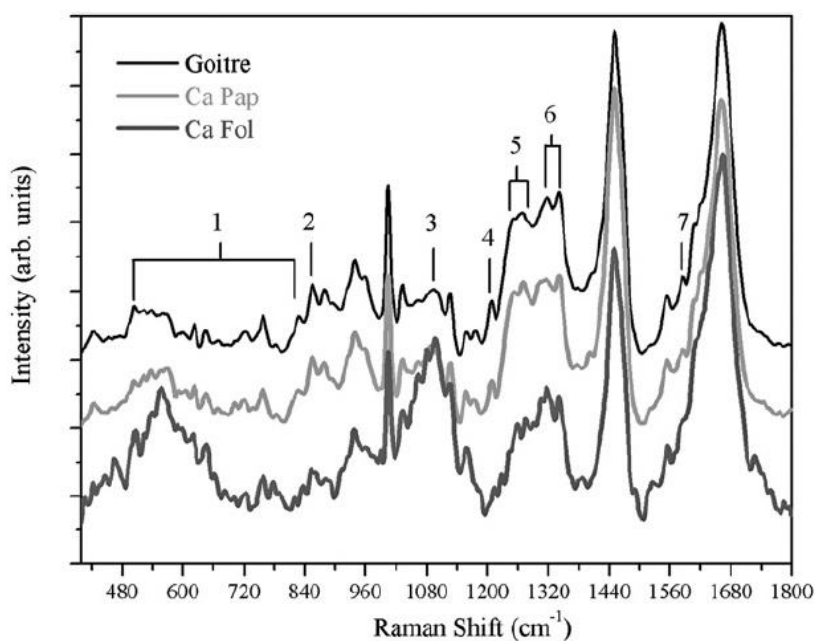


Fig. 17: Median of the adenomatous goitre spectra (black line), papillary carcinoma (grey line) and follicular carcinoma (dark grey line) (Layfield, Wax et al. 2003).

1.2.4 Limitations of Raman spectroscopy

However, although Raman spectroscopy is a highly sophisticated technique with a well-established ability to accurately discriminate neoplastic changes, there are several significant practical limitations.

A drawback of the technique is the long analysis time when spectral information is collected from an area other than points on a sample. The accuracy is clearly improved with longer acquisition times; also, point measurement systems require accurate placement of the clinical probes with low throughput.

Additional drawback is represented by the fact that interpretation and classification of Raman spectra requires complex multivariate algorithms. Thus, further developments in this field are aiding diagnostic models and it is hoped that

advanced data processing techniques, for example support vector machines and random forests, may improve diagnostic accuracy, although validation of these models is required prior to clinical implementation. In addition, future developments in probe design and construction may improve signal to noise ratios. Systems must be robust enough to withstand day-to-day usage by clinical staff and decontamination and disinfection processes.

1.2.5 Clinical application of Raman spectroscopy for thyroid cancer diagnosis

The diagnosis of thyroid pathologies usually occurs in the following order: anamnesis, ultrasonography and laboratory exams. Recently, a fine needle aspiration (FNA) could be required, where the cells collected are cytologically analyzed. From the FNA, if the suspected malignancy is confirmed, a surgical procedure (partial or total thyroidectomy) is advised so that, after the material is sent for histologic analysis (anatomical pathologic analysis), the medical diagnostic can be concluded. FNA is currently the most accepted procedure for diagnosing thyroid injuries, as it is a very useful and cost-effective tool. However, the sensitivity of this procedure for the thyroid is at times poor, with a high rate of false-negative results, and the variation ranges from 2% to 37% (Rout and Shariff 1999). The differentiation of hyperplastic nodule (goiter), follicular adenoma or follicular carcinoma is difficult. The accuracy of the method is doubtful in these cases, and other alternatives and further methods are necessary to make the diagnosis more precise for such obscure injuries to the cytopathologic diagnosis. False-negative



results occur due to an ordinary mistake in sampling, which may occur in small tumors and samples associated with inflammations and degenerative changes next to the thyroidal parenchyma. The cytopathologic diagnoses of follicular adenoma and follicular carcinoma are complicated because they depend on the histologic access to the capsular and vascular invasion perception. It is, therefore, vital to find new ways to detect the biochemical and cellular changes, in order to perfect the diagnosis and prognosis of thyroidal diseases. It is important to note that at times the incorrect diagnosis leads the patient to surgery without appropriate urgency and indication.

Considering the variations of the thyroid disease and the difficulty of the morphologic diagnosis, the necessity of further techniques to distinguish benign and malignant characteristics of the thyroid lesion is evident. It is known that these diseases, with no exception, are caused by biochemical changes in the cells and/or tissues. Thus, the current challenge of modern medicine is to find an analytic technique that investigates these alterations through minimally invasive and non-destructive methods. Few analytic methods fulfill these requirements and are sensitive enough to reveal details of the biochemical composition and structure (Bitar, Martinho Hda et al. 2006).

Among the new techniques recently presented, optical biopsy by Raman spectroscopy is one of the most promising ones, due to the biochemical alterations that can be detected by the optical spectroscopy through the disease's characteristic spectral signs. Different aspects could be detected by the Raman spectroscopy



method that can contribute and complement the clinic diagnosis of thyroidal
pathologies.

A handwritten signature in black ink, consisting of a stylized initial 'G' followed by a horizontal line that tapers to the right.

2. AIMS

- To determine the diagnostic accuracy of Raman spectroscopy in discriminate normal tissue, hyperplastic and neoplastic thyroid lesions through specific molecular fingerprints of healthy and pathological tissues on surgical specimens as well as on cytological samples.
- To delineate the specific molecular fingerprint of healthy and neoplastic benign and malignant tissues as possible marker for diagnosis to be applied in the clinical workup of thyroid nodule.
- To develop a portable diagnostic tool for clinical practice, using sterile fiber probes to be inserted into the nodule by needle, as devices for hospital use (optic biopsy).



3. Materials and methods

Patients' enrolment

This is prospective multicenter study approved by the Ethical Committee of the University of Campus Bio-Medico (UCBM) (prot. 33.15 TS ComEt CBM). From January 2018 to January 2020, we enrolled consecutive subjects with thyroid nodular pathology referred to the Endocrinology Unit of Campus Bio-Medico University Hospital (Tab. 1). All the study population had received a cytological diagnosis of indeterminate, suspicious or malignant lesion with a formal indication to surgery (total thyroidectomy) according to the international guidelines (Gharib, Papini et al. 2016). After signing the informed consent, these patients underwent total thyroidectomy at the Surgical Unit of the same Institution.

This study planned along different steps: 1. Enrolment of patients that received a diagnosis of thyroid nodules and that are candidate for undergoing surgery at the Endocrinology Unit of UCBM. 2. Performing of spectroscopy investigation by Raman microscopy intended to obtain numerous biochemical maps on ex-vivo thyroid tissues, each one containing elevated number of Raman spectra. A statistical analysis of the obtained data was performed, in order to generate tissue classification models. 3. Validation of the classification models by correlation with pathological data.



Exclusion Criteria for enrolment of patients were:

- Under 18 years of age
- Pregnant or lactating females
- Major mental comorbidity
- Concomitant other malignancy or within previous 5 years
- Previous chemotherapy or radiotherapy;
- Concurrent anticancer systemic therapy
- Suspicious for difficult assessment of pathological staging (margin involved in section).

A handwritten signature in black ink, consisting of a stylized initial 'G' followed by a horizontal line extending to the right.

Tab. 1 List of all the samples investigated by Raman Spectroscopy, along with clinical information. US Classification is done according to Tessler et al (Tessler, Middleton et al. 2017). Labels PTC, FV-PTC, FC, FA denote Papillary thyroid carcinoma, Follicular variant papillary thyroid carcinoma, Follicular thyroid carcinoma, Follicular thyroid adenoma, respectively. Label Oxy in the Histology diagnosis refers to Oncocytic variants. Label HTT refers to Hyalinizing Trabecular Tumor. Finally, N.A. means not applicable. The superscript ** labels the samples used to generate the reference Raman spectra reported in Fig. 21. Sample TIR59 is inadequate for Raman spectroscopy investigation: it was indeed too thin and the spectrum was dominated by the signal from the glass slide.

Samples	Gender	Age at diagnosis	US Classification (TI-RADS) ²⁴	Histology diagnosis	Raman Cluster	Immunocytochemistry diagnosis revision
TIR43	F	42	4	FA Oxy	FC	FA with altered markers
TIR44	M	62	3	FA	PTC	FA with altered markers
TIR45	F	77	4	PTC + FA Oxy	FC	PTC + FA Oxy
TIR46	F	42	5	PTC	PTC	
TIR47**	M	52	4	FC Oxy	FC	
TIR48	F	43	4	PTC Oxy	PTC	
TIR 49	F	45	4	PTC	PTC	
TIR50	F	30	5	PTC	PTC	
TIR51**	M	58	4	PTC	PTC	
TIR52	M	44	4	a) PTC b) FC	a)PTC b) FC	
TIR53	F	27	4	FA Oxy	Benign	
TIR55**	M	74	4	FC Oxy	FC	
TIR56**	F	43	4	FV-PTC	FV-PTC	FV-PTC
TIR57	F	47	4	FV-PTC	Benign	
TIR58**	F	38	4	PTC	PTC	
TIR59	F	32	4	FA Oxy	Inadequate	
TIR60	F	47	4	PTC	PTC	
TIR61	F	25	4	PTC Oxy	FC	PTC Oxy
TIR62	M	51	4	FA	Benign	
TIR63	F	31	3	FV-PTC	FV-PTC	
TIR64	F	65	3	FA	PTC	FA with micro PTC
TIR68	F	24	4	PTC	PTC	
TIR70	F	48	4	PTC	PTC	
TIR71	M	45	4	FA Oxy	FV-PTC	FA with altered markers
TIR72	F	32	4	PTC	PTC	
TIR73	F	58	4	HTT	PTC	HTT and PTC share common features
TIR74	M	39	3	FA Oxy	Benign	
TIR75	F	37	4	FV-PTC	PTC	FV-PTC
TIR76	F	42	5	PTC	FV-PTC	
TIR77	M	45	4	PTC	FV-PTC	
Hea 43	F	42	N.A.	Healthy	Healthy	
Hea46	F	42	N.A.	Healthy	Healthy	
Hea48	F	43	N.A.	Healthy	Healthy	
Hea49**	F	45	N.A.	Healthy	Healthy	
Hea50	F	30	N.A.	Healthy	Healthy	
Hea52	M	44	N.A.	Healthy	Healthy	
Hea56	F	43	N. A.	Healthy	FV-PTC	Near tumor area
Hea 57	F	47	N.A.	Healthy	Healthy	
Hea62	M	51	N.A.	Healthy	Healthy	
Hea63	F	31	N.A.	Healthy	FV-PTC	Near tumor area
Hea64**	F	65	N.A.	Healthy	Healthy	
Hea68	F	24	N.A.	Healthy	Healthy	
Hea70	F	48	N.A.	Healthy	Healthy	
Hea72	F	32	N. A.	Thyroiditis/Benign	FV-PTC	Near tumor area
Hea76	F	42	N.A.	Healthy	Healthy	

Thyroid tissue preparation

Patients afferent to the Endocrinology Unit of Campus Bio-Medico for thyroid nodular pathology were evaluated by clinical and ultrasonography examination and submitted to fine needle aspiration biopsy when appropriate (Gharib, Papini et al. 2016). Those who received a cytological diagnosis of indeterminate, suspicious or malignant lesion and an indication to surgery were enrolled for the study. These patients underwent total thyroidectomy at the Surgical Unit of the same Institution (Figure 18-19). At the time of surgery, the removed specimens were immediately submitted unfixed to the Pathology Unit in an appropriately labeled container. The pathologist valued the gross anatomy of the samples and a tissue slice of about 1 cm wide x 1 cm length x 3 mm of thickness, was cut, including both healthy and neoplastic areas, avoiding surgical margins. The slice was snap frozen on a metallic cold-plate inside a cryostat. A 5 μ m section was stained with haematoxylin/eosin in order to confirm the presence of healthy and neoplastic tissues. After this step, four consecutive cryostatic sections were cut at 30 μ m and two section at 15 μ m of thickness, collected on separate slides and stored at -80°C until the Raman and enzymatic evaluation. The residual slices were defrosted, formalin fixed, and paraffin embedded with the paired surgical samples for definitive histology. Final diagnosis was reported in agreement with current edition of WHO classification of endocrine Tumors. Immunohistochemical analysis for Galectin3, CK19, CD56 and HBME1 was performed in each case on paraffin sections from neoplastic areas using an automatized immunostainer (Omnis, Agilent).



Nodules with diameter wider than 2 cm were submitted for biochemical analysis.

In such cases, at the time of gross dissection, further slices of about 0,5 x 0,5 cm were cut from the surgical specimen, sampling both healthy and neoplastic tissue.

Slices were snap frozen and stored at -80°C until biochemical evaluation.

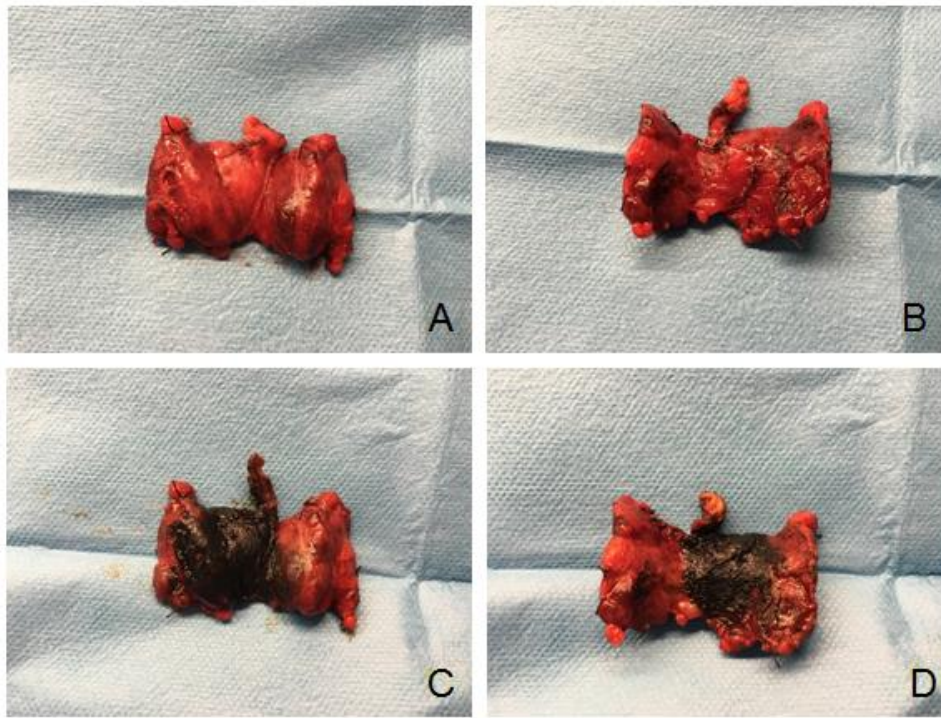


Fig. 18: Thyroid tissue preparation of a PTC located in right lobe. (A) Frontal view of surgical specimen. (B) Posterior view of surgical specimen. Resection margins were marked with black ink in the front (C) and in the back (D).

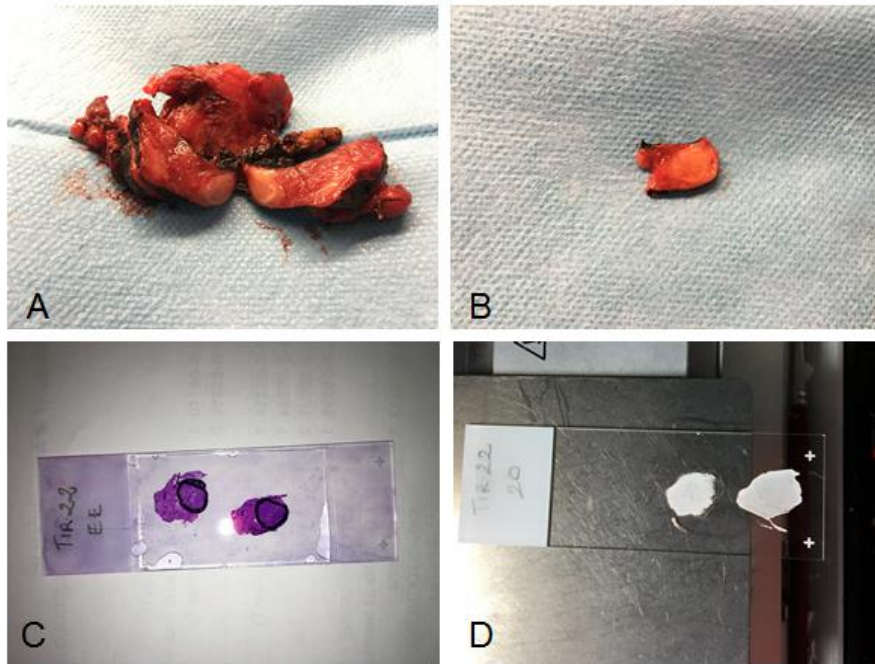


Fig. 19: (A) The PTC is located in the right lobe. (B) A tissue slice of about $1 \times 1 \times 0.3 \text{ cm}^3$ including both healthy and neoplastic areas. (C) A cryostatic section stained with Haematoxylin/Eosin (D) Cryostatic sections cut a $30 \mu\text{m}$ of thickness for Raman evaluation.

Raman spectroscopy

Raman spectra and statistical analysis were carried out at Science Department of University “Roma tre” (data are under publication, Sbroscia M. et al; Thyroid Cancer Diagnosis by Raman Spectroscopy, 2020). Spectra have been collected by means of a Renishaw InVia Micro-Raman spectrometer. In this set-up unpolarised spectra are collected through a Leica DM2700 M confocal microscope equipped with a Leica 50X LWD and an Olympus 100X objective. The required high-contrast rejection for the elastically scattered light is provided by a holographic edge filter. A diffraction grating with 1800 grooves/mm disperses the Raman inelastic

A handwritten signature in black ink, consisting of a stylized initial 'G' followed by a horizontal line.

scattering contribution providing a spectral resolution of about 1 cm^{-1} . A Peltier cooled 1024×256 pixel CCD detector collects the dispersed light. A solid-state diode laser source at 532 nm with a nominal output power of nearly 60 mW has been used as excitation source. To prevent photo-damage, neutral density filters have been used for lowering the laser power at the sample. The spot size has been shrink down to few microns when necessary to isolate the contribution of cells (about ten microns in size) from the surrounding cytoplasm, thus reducing spectral interference. Spectra have been collected in the extended scan mode, covering the $100 - 3800 \text{ cm}^{-1}$ frequency shift range and accumulating 5 scans with an equivalent integration time of nearly 10 seconds per scan. Wire (Renishaw) software has been used to collect the raw spectra. Wire and LabSpec software has been used to perform the preliminary data reduction (e.g. background and fluorescence subtraction), while Origin (OriginLab Corporation) software has been employed to perform the statistical analysis. After background and fluorescence subtraction, all the spectra have been normalized to their integral, in order to avoid any bias due to fluctuations of the experimental conditions.

Cluster analysis of Raman spectra

In order to statistically analyze the RS data, we have selected two unsupervised multivariate statistical approaches to analyze the Raman spectra: the agglomerative hierarchical clustering analysis (AHCA) and the K-means one (KM). Both methods are based on the Euclidean distance among spectra, as a measure of their similarity/dissimilarity. In detail, in these analyses, spectra are represented by their



distance with respect to an origin, thus generating a dissimilarity matrix. Among the possible choices for the spectral distance, the Euclidean one was selected in order to maximize the similarities among the spectra. The choice to use these two methods was made to exploit their complementarity of hierarchical and non-hierarchical approaches and consequently to give solidity to the obtained results (Koljenovic, Schut et al. 2005, Harris, Garg et al. 2009, Teixeira, Bitar et al. 2009, Pereira, Zezell et al. 2013).

The AHCA method aims to classify observations (each Raman spectrum) into homogeneous groups (the clusters) based on the measured characteristics (Euclidean distance associated to each Raman spectrum). In particular, the complete-linkage algorithm was used to enhance differences among clusters. It works by pairing the most similar spectra (those showing the lowest dissimilarity value in the matrix) and then looking for the largest distance between such pair and the rest of the data. By iteratively repeating such an approach, a classification of spectra into well-separated groups is obtained and visualized as a dendrogram.

The KM method minimizes the variance within each cluster with respect to a priori number of centroids, randomly distributed. This protocol starts by associating each data entry (Euclidean distance associated to each Raman spectra) to the cluster with the closest centroid. The centroids are iteratively updated and the process goes towards convergence. In order to choose the proper value of k , the most used strategy is the “elbow curve”, based on the explained variance within the entire dataset. This analysis, in our case, gives only two centroids; one for samples containing mainly carotenoids and one for all other cases. Thus following the



suggestion of the histology diagnosis, we have set $k=4$. In order to verify the reliability of this choice, the spread of each cluster was calculated compared to its centroid as a function of k . $k=4$ is resulted as the highest k -value with the lowest spread (shown in Fig.20).

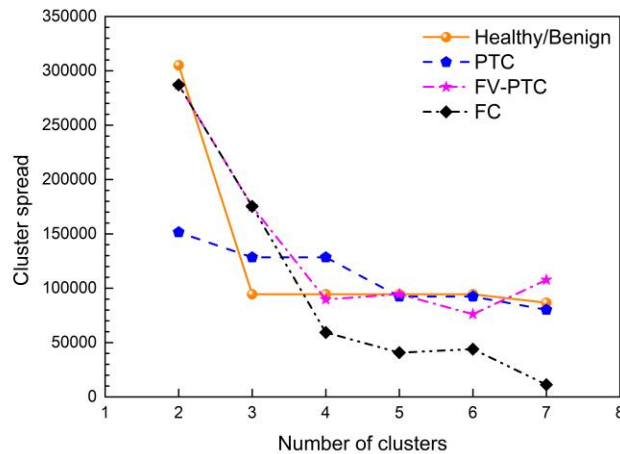


Fig. 20: Spread of the individual K-means clusters as a function of their number.

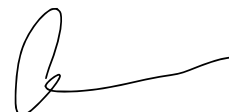
The predictive accuracy of both AHCA and KM methods were tested by generating a confusion matrix. This allows the comparison between the medical diagnosis and spectroscopic evaluation. The accuracy is defined as: $[\text{True negative} + \text{True positive}] / \text{number of total samples}$.

Biochemical analysis

Frozen thyroids were weighted, homogenized and sonicated in lysis buffer (20 mM Tris-HCl pH 8.0, 137 mM NaCl, 10 mM EDTA, 10% glycerol (v/v), 1% TritonTM

X-100 (v/v), and protease inhibitors). Twenty-five micrograms of protein extracts, previously quantified with the Bradford assay (Bio-Rad, Hercules, CA), were resolved by 15% SDS-PAGE and transferred onto PVDF membranes (Bio-Rad). After blocking with 3% BSA (w/v) dissolved in TBS buffer/ 0.5% Tween-20 (v/v), membranes were probed overnight at 4 C with anti-cytochrome *c* (mouse mAb, sc-13560; Santa Cruz Biotechnology, Dallas, TX, USA) and anti-actin (mouse mAb, sc-47778; Santa Cruz Biotechnology) primary antibodies. Membranes were then incubated for 1 h at room temperature with an anti-mouse HRP-conjugated secondary antibody (Bio-Rad). All the experiments were repeated twice. Blots were acquired and processed using the ChemiDoc™ Imaging system (Bio-Rad). Cytochrome *c* quantification was performed using the Image Lab software (version 6.0.1, Bio-Rad Laboratories). Results are shown as mean standard deviation (SD); the statistical significance of differences was tested using the Student's t-test (GraphPad Prism, version 6.01).

Biochemical analysis are carried out at Science Department of University "Roma Tre".



4. Results and Discussion

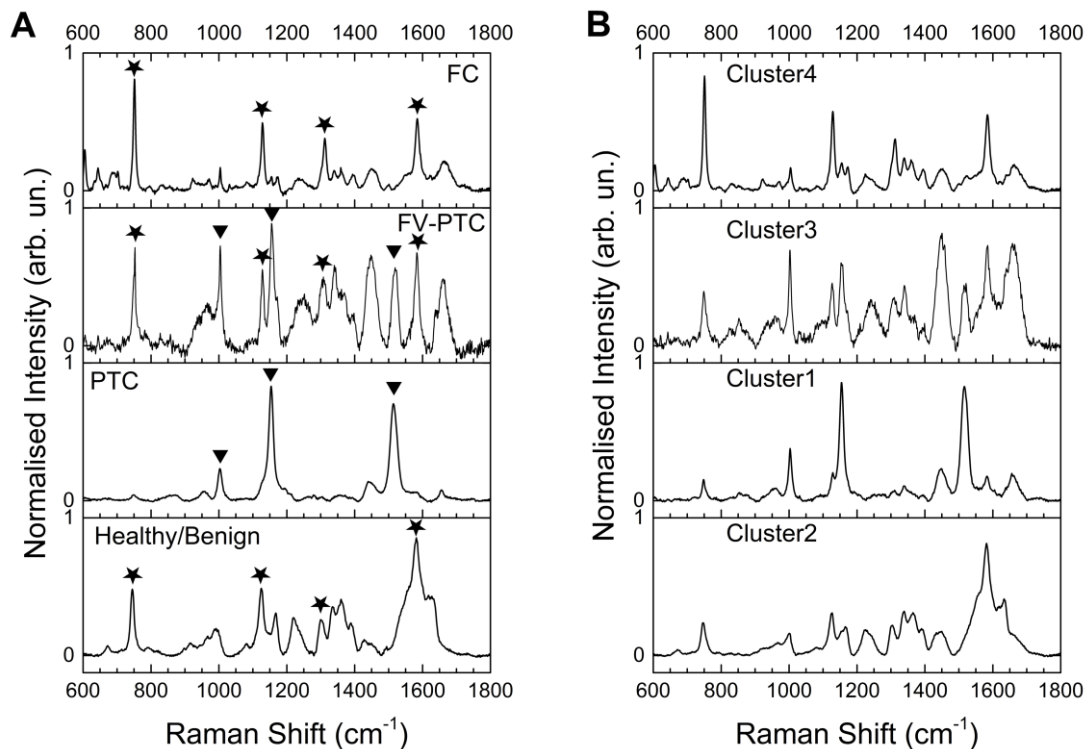


Fig. 21: A) Typical Raman spectra of the examined thyroid tissues, labeled according to the histology report. Stars label the Raman peaks characteristic of cytochrome *c*, triangles those of carotenoids. B) Raman spectra of the centroids of the K-means analysis, for the four identified clusters.

Figure 21A shows the Raman fingerprint region (600 - 1800 cm^{-1}) of four samples with a clear histology diagnosis, namely Healthy/Benign, PTC, FV-PTC and FC carcinoma tissues, from bottom to top. Each spectrum has been normalized to its integrated intensity. Each tissue shows its own characteristic spectral line shape. According to Rau et al (Rau, Graziani et al. 2016).

The spectrum of the healthy tissues is dominated by an intense, broad and structured band centered around $\sim 1600\text{ cm}^{-1}$, possibly due to the presence in the sample of amide I and lipids. The sharpest structure of this band falls at 1582 cm^{-1} and along with the bands at 747 , $1120 \div 1128$, and 1301 cm^{-1} represents the fingerprint of cytochrome *c* (Marshall, Leuko et al. 2007, di Masi, Leboffe et al. 2019). This is a protein localized in the mitochondrial intermembrane space under normal physiological conditions. The spectrum of a classical papillary carcinoma (labeled PTC in Fig.21A) is totally different and unambiguously shows the presence of carotenoids (bands at 1003 , 1155 and 1516 cm^{-1}), not present in healthy tissues, as already reported in the literature (Marshall, Leuko et al. 2007, Teixeira, Bitar et al. 2009, Rau, Fosca et al. 2017). In the spectrum of the follicular carcinoma (labeled FC in Fig.21A) is observed a marked enhancement of the cytochrome *c* bands. After spectral intensity normalization, the broad band at $\sim 1600\text{ cm}^{-1}$ that dominates the Healthy/Benign spectra is barely visible in this case. Interestingly, the spectrum of the Papillary Follicular carcinoma (labeled FV-PTC in Fig. 21A) looks like a superposition of the PTC and FC spectra, showing the fingerprints of carotenoids and cytochrome *c*.

The presence of carotenoids in both PTC and FV-PTC carcinoma is peculiar and worth of interest: indeed the process of cellular uptake of carotenoids (not directly synthesized by human organisms) and their proper identification is under biochemical investigation.



46 histological samples of human thyroid were studied: 15 samples was healthy, 8 adenomas, 16 PTC, 4 FV-PTC, 3 FC. Within each histology class, spectra may differ for noise, background or fluorescence contributions, although keeping unaltered the characteristic fingerprints. This observation suggests that the experimental spectra can be analyzed on quantitative grounds, after background and fluorescence subtraction, by a cluster analysis. Raman spectra were classified into homogeneous groups, based on its characteristic features such as presence and relative intensity of specific bands.

The AHCA analysis is a method of cluster analysis that seeks to build a hierarchy of clusters by agglomerative approach. The results build a dendrogram of the entire data set, by iteratively selecting pairs of the closest spectra or groups of spectra as a function of their Euclidean distance (Fig. 22). The spectra are consistent with a classification of the dendrogram into 4 clusters, assuming a distance threshold of 0.58 to be compared with a maximum distance of 1.05. The four clusters have been labeled according to the results reported in Fig.21. The Healthy/Benign and PTC spectra are very well distinct each other and have the smallest dispersion in terms of Euclidean distance within each clusters. Smaller dispersion of the Euclidean distances results in a better homogeneity of the group: in the present case Healthy/Benign and PTC tissues are the most homogeneous. The other two clusters (FC and FV-PTC) are more dispersed, although equally distinguishable from the others. The FC cluster is the closest to the Healthy/Benign one: both are characterized by the presence of cytochrome c but distinguished only on the basis of its Raman fingerprint relative intensity. The FV-PTC spectra tissues fall between



FC and PTC clusters, cause both are characterized by the presence of carotenoids and cytochrome c.

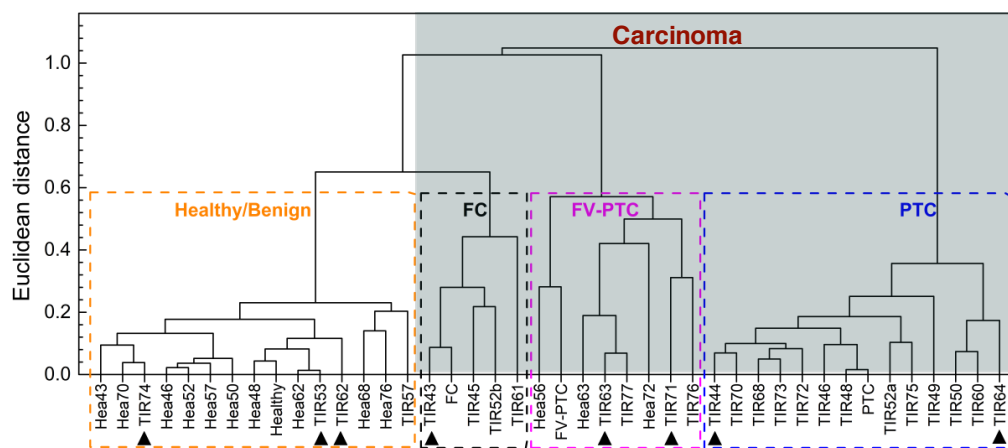


Fig. 22: Agglomerative Hierarchical Clustering Analysis. Dendrogram of the Raman spectra of human thyroid tissues, as extracted from the AHCA analysis. Individual samples are represented by the label Hea (for healthy), or TIR (for not healthy) followed by the patient anonymous ID code. Those plotted in Fig. 21A are labelled Healthy, FC, FV-PTC and PTC, respectively. Dashed squares identify the four clusters, namely Healthy/Benign (orange), Follicular carcinoma or FC (black), Follicular variant of Papillary carcinoma or FV-PTC (magenta) and Papillary carcinoma or PTC (blue). The arrows indicate the adenoma samples. All samples within the light blue shaded area are carcinoma.

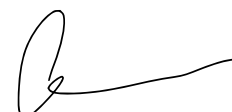
The second unsupervised statistical approach considered is K-means (KM) reported in Fig.23. This confirms that four clusters properly describe our data set. Clusters 1, 2, 3, 4 contain samples from the histology reports of PTC, Healthy/Benign, FV-PTC and FC, respectively. The agreement between the clustering results of the two approaches is very good. In this second statistical analysis, the only sample that switches from PT to FV-PTC is TIR60. The Raman spectrum of TIR60 is borderline between the two clusters; it is possible that the two methods (AHCA and K-means)

place TIR60 in two different but close clusters, based on its Euclidean distance.

Fig.23 shows that Healthy/Benign tissues spectra have the shortest distance from their centroid and the smallest dispersion. On the contrary, the spectra of FV-PTC tissues are the most dispersed, possibly due to a different balance of concentration between carotenoids and cytochrome c in each sample. Table 2 reports the distance matrix among the clusters centroids. Cluster 1, showing the largest centroid distance from the others, is readily isolated (Raman spectrum is dominated by the carotenoid fingerprint), while discrimination among the others requires considerations from more spectral details.

Tab. 2: Euclidean distance between the cluster centers.

	Cluster 1	Cluster 2	Cluster 3	Cluster 4
Cluster 1	0	24611	19319	24211
Cluster 2	24611	0	13539	14249
Cluster 3	19319	13539	0	14117
Cluster 4	24211	14249	14117	0



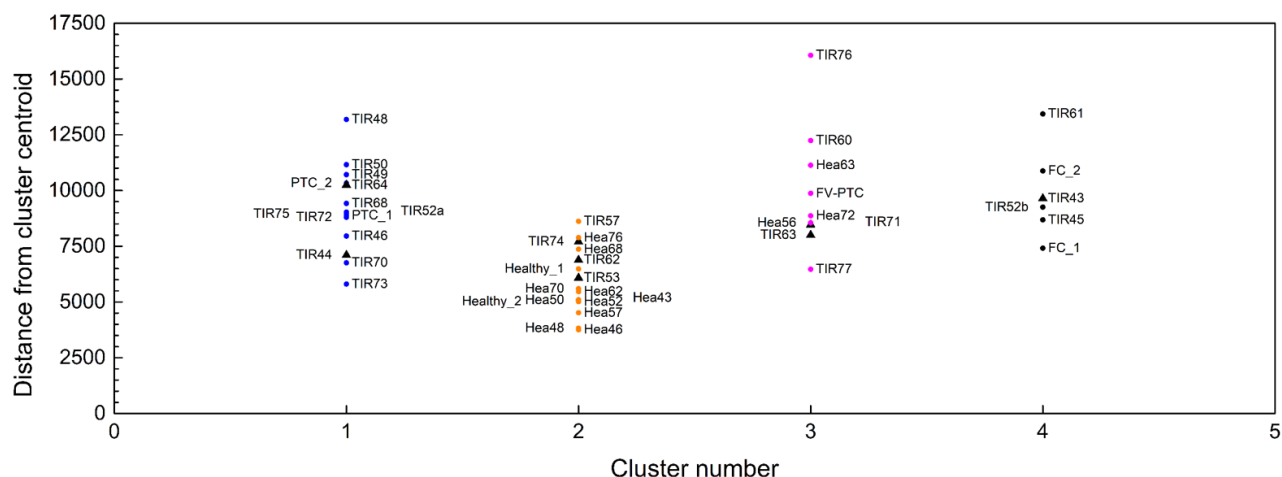


Fig. 23: Samples distribution within the four KM clusters, as a function of their Euclidean distance from the associated centroid. The same labels and colors as in Fig.22 have been used. Black triangles refer to adenomas.

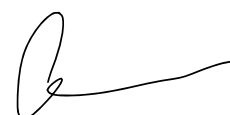
The Raman spectra calculated for each cluster centroid (Fig.21B) by KM analysis overlap the prototypical spectra of the four tissue classes (Fig.21A). The similarity of the spectra reported in Fig. 21A and B is astonishing and proves that our clustering is solid.

Based on these results, a confusion matrix has provided the accuracy of our analysis to discriminate between Healthy/Benign and carcinoma tissues, and among the three categories of carcinoma (PTC, FC, FV-PTC). As reported in Tab.2, our accuracy is of ~90%.

Tab. 3: Confusion matrix based on 38 samples (healthy and carcinomas tissues). This shows that RS has identified 1 false negative diagnosis among the 15 negative Medical diagnosis and 3 different samples among the 23 with a positive diagnosis, which fall in a cluster different from those expected on the basis of the medical diagnosis.

Total of 38 samples	Raman	Classification	Accuracy
Medical diagnosis	True negative 12 False negative 1	False positive 3 True positive 22	0.90

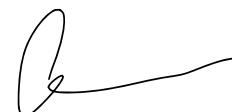
The same analysis is applied including the spectra of the samples classified as adenoma by the histological diagnosis. Their position is highlighted by arrows in the AHCA dendrogram of Fig.22 and in the distributions of Fig.23. These figures show that the spectra of adenoma tissues spread over all four clusters defined by healthy and cancerous tissues. This is a quite unexpected result, as adenomas are classified as benign tissues and therefore should fall into the Healthy/Benign cluster. Accordingly, the confusion matrix after inclusion of adenoma samples, reported in Table 4, returns an accuracy of the statistical analysis of 82%.



Tab. 4: Confusion matrix based on 45 samples (including adenomas). This shows that RS has identified 1 false negative diagnosis among the 15 negative Medical diagnosis and 7 different samples among the 29 with a positive diagnosis, which fall in a cluster different from those expected on the basis of the medical diagnosis.

Total of 45 samples	Raman	Classification	Accuracy
Medical diagnosis	True negative 15 False negative 1	False positive 7 True positive 22	0.82

The RS analysis revealed four adenoma samples, TIR43, TIR44, TIR64 and TIR71, that fall within the cancerous clusters. These data have been in depth reanalyzed as far as their expression of benignity and cancerous markers are concerned, by immunohistochemistry test (IHC). The IHC staining with anti- CD56, anti- Galectin3 and anti-HBME1 revealed either the lowering of benignity markers (CD56), or sometimes the onset of tumoral markers (Galectin3, HBME1), as shown in Fig.24. These results could be symptomatic of early stages of progression of adenomas into a specific type of carcinoma. Such type of transformation has never been demonstrated, suggesting that Raman spectroscopy could become relevant in these samples, allowing an early identification of benign tumors with a possible malignant behavior. Our Raman observation opens a new light about the malignant potential of thyroid adenoma and about the possibility to assess which of these lesions may constitute a clinical concern.



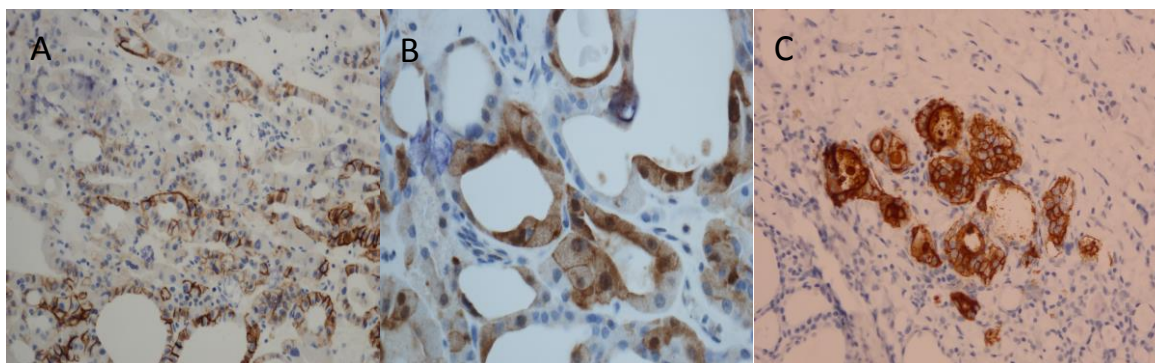
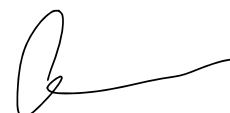


Fig. 24: Microscopic pictures A and B) TIR43 sample stained with immunohistochemistry for CD56 (A) and galectin3 (B). CD56 showed sparse cells with loss of normal membrane staining. Consecutive paraffin section from the same case showed cells with positive staining for the neoplastic marker Galectin3. Positive and negative cells are intermingled in a mosaic pattern, suggesting an incomplete, possibly ongoing, cellular transformation. (High power field. Hematoxylin counterstained). C) TIR64 sample stained with immunohistochemistry for HBME1. A strongly positive cluster of cells indicates a microscopic focus of papillary carcinoma within an adenoma nodule. This finding was supported by morphological examination. (Medium power field. Hematoxylin counterstained).

A few anomalies, visible in Fig.22 and 23, deserve a comment. Sample Hea56 and sample Hea63 apparently fall into a wrong cluster, namely the FV-PTC cluster, but interestingly very close to their TIR counterpart (FV-PTC and TIR63, respectively). This may happen when the Raman spectrum of the healthy portion is collected from a tissue region too close to the pathologic one. The case of sample Hea72, falling within the FV-PTC cluster, may be due to the diffusion of carotenoids in normal parenchyma at the border of the PTC nodule, as already observed in previous Raman chemigram map of thyroid carcinomas (Rau, Graziani et al. 2016). This gives in the Raman spectrum the superposition of the fingerprint of carotenoids with



fingerprint of healthy tissues (containing cytochrome *c*), thus explaining the "wrong" assignment obtained by Raman analysis.

Additionally, levels of cytochrome *c* have been further evaluated by biochemical analysis (Fig.25) on a few cases. Indeed, only for patients 44, 46 and 48 (PTC), and 45 and 47 (FC) a sufficient amount of thyroid tissue was available to perform immunoblot analyses. As shown in Fig.25, cytochrome *c* levels significantly increase in TIR45 (13.4-fold induction compared to its healthy counterpart Hea45; $P < 0.01$), TIR46 (2.7-fold induction compared to Hea46; $P < 0.05$), and TIR47 compared to their healthy counterparts (Hea) ($P < 0.01$). In agreement with Raman results, cytochrome *c* levels are similar in TIR and Hea slices of patients 44 and 48.



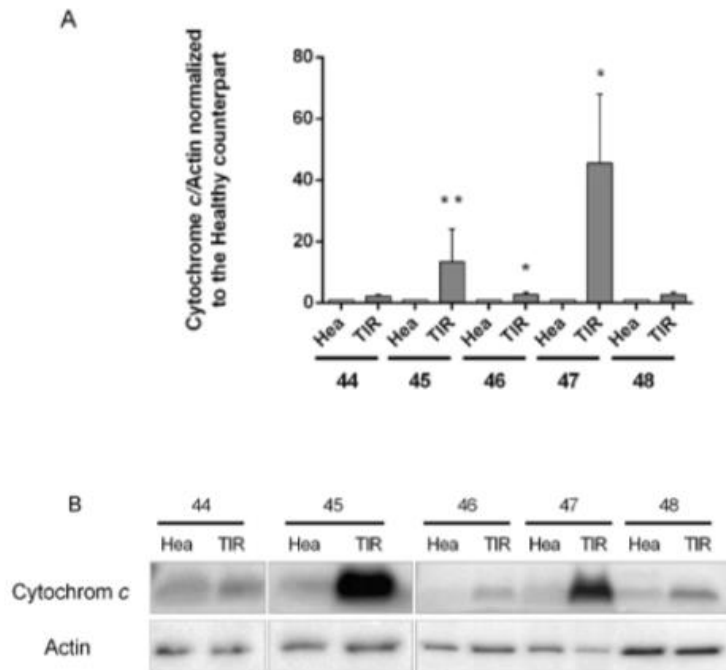


Fig. 25: Expression levels of cytochrome c were assessed in thyroids of five patients; for each patient, the healthy (Hea) and pathological (TIR) slices were analysed. (A) Levels of cytochrome c were normalized to actin. Data represent the mean values \pm SDs derived from two replicates normalized to healthy counterparts (Student's t test, * $P < 0.05$, ** $P < 0.01$ compared with control). (B) Exemplificative images of filters blotted with cytochrome c and actin primary antibodies. Images have been gathered at the same time.


5. Conclusion

Our results have demonstrated the feasibility and reproducibility of RS to discriminate healthy/benign thyroid tissue from PTC, FC and FV-PTC based on their biochemical fingerprints.

Based on the experimental results obtained in this work, we can attest the significant carotenoids presence in the PTC tissues and the overexpression of cytochrome *c* in FC samples with respect to the healthy tissue.


In our study, we considered range of thyroid Raman spectra, both presenting changes while passing from healthy to PTC to FC and to FV-PTC areas and, therefore, both important for diagnostic utility, as confirmed also by authors for cervical tissue (Duraipandian, Zheng et al. 2012).

RS has the ability to identify specific tumor expression molecules and molecular species involved in tumorigenesis and progression. For instance, Talari et al (Talari, Movasaghi et al. 2015) claimed the 956, 1006, 1156-1157, 1524-1528 cm^{-1} Raman peaks as “carotenoids absent in normal tissue”. Puppels et al. (Puppels, Garritsen et al. 1993) investigated carotenoids located in human lymphocyte subpopulations and natural killer cells, evidencing a high carotenoids concentration in the CD4^+ lymphocytes, and proposed to investigate the possible mechanisms behind the protective role of carotenoids against the development of cancers. The increased intensities at 1159 and 1527 cm^{-1} , assigned to carotenoids have been identified also in the Raman spectra of brain tumors and neurinomas (Mahadevan-Jansen and Richards-Kortum 1996, Talari, Movasaghi et al. 2015). Talari et al. suggested that carotenoids could be used as Raman biomarkers in breast cancer pathology.



The coupled histopathological and Raman biochemical observations performed in this work highlighted that carotenoids are mainly present in cellular areas of PTC and cytochrome *c* are present in FC, so that their presence seems to be related to the neoplastic thyrocytes within the tumor tissue. Our study suggests that these characteristics could be used as Raman biomarkers in the thyroid carcinoma pathology. However, the mechanism underlying potential oncogenic effects of carotenoids is still unknown, since very little is known about the biochemical content of neoplastic cells especially what regards lipids, lipoproteins and lipophilic substances that are commonly lost in routinely processed histological samples. Among human tissues, different normal cells are able to utilize carotenoids, i.e. beta-carotene is reported as a local supply of vitamin A in the skin and melanocytes (Andersson, Vahlquist et al. 2001). However, physiological mechanism for carotenoids uptake in normal thyrocytes is not reported, and our results raise the hypothesis of a carotenoid-related pathway for the PTC oncogenesis. This hypothesis needs for validation but underlines the presence of carotenoids in neoplastic thyrocytes, as previously described for other organs.

Only a few literature studies report RS investigations of thyroid tissue and neoplasia (Teixeira, Bitar et al. 2009). The particularity of our RS analysis is that for the first time it is performed on tissue sections and combined with microscopic assessment of the analyzed areas. The method is very cost-effective, being the cryostatic tissue sections observed without any additional staining or treatment. Our results represent a major advance in imaging of thyroid tissues, leading to subsequent clinical application of the RS diagnostics. As a potential clinical tool to support cancer



diagnosis, RS should improve clinical accuracy in decision-making and reduce inter-observer variability.

This study is the first demonstration of particular features of the spectroscopic fingerprint of the PTC, FC and FV-PTC tissues presenting the significant presence of different molecules with respect to the healthy tissue. Our investigation suggests that carotenoids and cytochrome *c* could be used as Raman biomarker for the thyroid lesion. With this regard, combination of the histological and Raman microscopy analysis approaches should open a new way to integrative findings with wide implications for basic pathobiology, tumor classification schemes, and therapeutic strategies.

Assessment of risk of malignancy (ROM) in thyroid nodules is key to improved care. To assess ROM, medical history, physical examination, the results of ultrasound (US)-guided fine needle aspiration biopsy (FNA) are used. Molecular test could be diagnostic when used for thyroid nodules or prognostic in thyroid cancer but the main limitation is that the tests are not widely available, particularly worldwide. Their cost is relatively high, especially outside the US. In addition, their positive predictive value is low, which means that when the test is positive, many nodules may not be malignant. The researchers found that gene alterations appeared in only 50% of the cancerous samples (ie, 50% sensitivity) and 20% of the benign thyroid samples harbored gene alterations (ie, 80% specificity). These data suggest that the molecular test lacked accuracy in ruling cancer in or out because gene mutations were found in both benign and malignant samples and similarly were not present in both types of samples. Our Raman and histological data evidenced only



one false negative, giving a 97% of accuracy in ruling cancer out. In this landscape, if our results of Raman spectroscopy clustering for histological tissues will be confirmed in cytological samples obtained by FNA technique, this method could be more sensitive than molecular tests that lack similar accuracy in ruling cancer out. Moreover, Raman spectroscopy is a label-free technique, so the procedure is inexpensive out of the acquisition of the instrument and shows a strong economic advantage when compared with molecular tests.

In conclusion, this study demonstrates the capability of Raman spectroscopy as diagnostic tool for thyroid cancer. Based on data from 45 neoplastic histological samples and their benign counterparts, we identified a specific Raman spectra for the most common thyroid pathologies. Indeed, through statistical analysis of the spectra it is possible to readily separate healthy from cancerous tissues and discriminate among the most common cancer typologies. Our findings put into evidence the possible use of Raman spectroscopy as a tool for pre-surgical diagnosis of thyroid pathology by applying the method on cytological samples. Finally, yet importantly, our results open the way to a possible application of in vivo of Raman analysis without tissue sampling, through the introduction of a miniaturized optical fiber directly into the nodule.

Several future perspectives can derive from these preliminary results:

1. The development of a RS optical biopsy system to investigate in situ thyroid tissue alterations. This innovative diagnostic device should be represented by a needle containing the RS fibers to explore in vivo thyroid nodules and to perform in situ optical biopsy by Raman spectra without sampling the lesion.



2. The development of intraoperative technology which may be able to classify cell populations in real time, making it an ideal guide for surgical resection and decision making. Raman-based probe could be used, for example, to define surgical margin during thyroid surgery, to evaluate nodes involvement allowing to perform the correct modality of lymphadenectomy, to evaluate the presence of surgical residual after thyroidectomy.
3. Finally, the complex and huge amount of molecular information obtained by Raman spectra analysis of thyroid cancer may be the basis for a better knowledge of thyroid cancer oncogenesis. Raman spectra in fact showed a modulation of cytochrome enzyme expression and carotenoids cellular uptake that are currently under investigation and are apparently unrelated to the known genetic alteration landscape of thyroid cancer. This approach may open a new understanding of thyroid oncogenesis.



REFERENCES

Alexander, E. K., G. C. Kennedy, Z. W. Baloch, E. S. Cibas, D. Chudova, J. Diggans, L. Friedman, R. T. Kloos, V. A. LiVolsi, S. J. Mandel, S. S. Raab, J. Rosai, D. L. Steward, P. S. Walsh, J. I. Wilde, M. A. Zeiger, R. B. Lanman and B. R. Haugen (2012). "Preoperative diagnosis of benign thyroid nodules with indeterminate cytology." N Engl J Med **367**(8): 705-715.

Andersson, E., A. Vahlquist and I. Rosdahl (2001). "Beta-carotene uptake and bioconversion to retinol differ between human melanocytes and keratinocytes." Nutr Cancer **39**(2): 300-306.

Are, C. and A. R. Shaha (2006). "Anaplastic thyroid carcinoma: biology, pathogenesis, prognostic factors, and treatment approaches." Ann Surg Oncol **13**(4): 453-464.

Aschebrook-Kilfoy, B., R. H. Grogan, M. H. Ward, E. Kaplan and S. S. Devesa (2013). "Follicular thyroid cancer incidence patterns in the United States, 1980-2009." Thyroid **23**(8): 1015-1021.

Baker, R., P. Matousek, K. L. Ronayne, A. W. Parker, K. Rogers and N. Stone (2007). "Depth profiling of calcifications in breast tissue using picosecond Kerr-gated Raman spectroscopy." Analyst **132**(1): 48-53.

Barroso, E. M., R. W. Smits, T. C. Bakker Schut, I. ten Hove, J. A. Hardillo, E. B. Wolvius, R. J. Baatenburg de Jong, S. Koljenovic and G. J. Puppels (2015). "Discrimination between oral cancer and healthy tissue based on water content determined by Raman spectroscopy." Anal Chem **87**(4): 2419-2426.

Bartolazzi, A., F. Orlandi, E. Saggiorato, M. Volante, F. Arecco, R. Rossetto, N. Palestini, E. Ghigo, M. Papotti, G. Bussolati, M. P. Martegani, F. Pantellini, A. Carpi, M. R. Giovagnoli, S. Monti, V. Toscano, S. Sciacchitano, G. M. Pennelli, C. Mian, M. R. Pelizzo, M. Ruge, G. Troncone, L. Palombini, G. Chiappetta, G. Botti, A.



Vecchione, R. Bellocco and G. Italian Thyroid Cancer Study (2008). "Galectin-3-expression analysis in the surgical selection of follicular thyroid nodules with indeterminate fine-needle aspiration cytology: a prospective multicentre study." Lancet Oncol **9**(6): 543-549.

Beaudenon-Huibregtse, S., E. K. Alexander, R. B. Guttler, J. M. Hershman, V. Babu, T. C. Blevins, P. Moore, B. Andruss and E. Labourier (2014). "Centralized molecular testing for oncogenic gene mutations complements the local cytopathologic diagnosis of thyroid nodules." Thyroid **24**(10): 1479-1487.

Bergholt, M. S., W. Zheng and Z. Huang (2013). "Development of a multiplexing fingerprint and high wavenumber Raman spectroscopy technique for real-time in vivo tissue Raman measurements at endoscopy." J Biomed Opt **18**(3): 030502.

Bergner, N., B. F. Romeike, R. Reichart, R. Kalff, C. Krafft and J. Popp (2013). "Tumor margin identification and prediction of the primary tumor from brain metastases using FTIR imaging and support vector machines." Analyst **138**(14): 3983-3990.

Bignell, G. R., F. Canzian, M. Shayeghi, M. Stark, Y. Y. Shugart, P. Biggs, J. Mangion, R. Hamoudi, J. Rosenblatt, P. Buu, S. Sun, S. S. Stoffer, D. E. Goldgar, G. Romeo, R. S. Houlston, S. A. Narod, M. R. Stratton and W. D. Foulkes (1997). "Familial nontoxic multinodular thyroid goiter locus maps to chromosome 14q but does not account for familial nonmedullary thyroid cancer." Am J Hum Genet **61**(5): 1123-1130.

Bitar, R. A., S. Martinho Hda, C. J. Tierra-Criollo, L. N. Zambelli Ramalho, M. M. Netto and A. A. Martin (2006). "Biochemical analysis of human breast tissues using Fourier-transform Raman spectroscopy." J Biomed Opt **11**(5): 054001.

Brito, J. P., A. Al Nofal, V. M. Montori, I. D. Hay and J. C. Morris (2015). "The Impact of Subclinical Disease and Mechanism of Detection on the Rise in Thyroid Cancer



Incidence: A Population-Based Study in Olmsted County, Minnesota During 1935 Through 2012." Thyroid **25**(9): 999-1007.

Brito, J. P., M. R. Gionfriddo, A. Al Nofal, K. R. Boehmer, A. L. Leppin, C. Reading, M. Callstrom, T. A. Elraiyah, L. J. Prokop, M. N. Stan, M. H. Murad, J. C. Morris and V. M. Montori (2014). "The accuracy of thyroid nodule ultrasound to predict thyroid cancer: systematic review and meta-analysis." J Clin Endocrinol Metab **99**(4): 1253-1263.

Cabanillas, M. E., D. G. McFadden and C. Durante (2016). "Thyroid cancer." Lancet **388**(10061): 2783-2795.

Canzian, F., P. Amati, H. R. Harach, J. L. Kraimps, F. Lesueur, J. Barbier, P. Levillain, G. Romeo and D. Bonneau (1998). "A gene predisposing to familial thyroid tumors with cell oxyphilia maps to chromosome 19p13.2." Am J Hum Genet **63**(6): 1743-1748.

Cavaco, B. M., P. F. Batista, C. Martins, A. Banito, F. do Rosario, E. Limbert, L. G. Sobrinho and V. Leite (2008). "Familial non-medullary thyroid carcinoma (FNMTTC): analysis of fPTC/PRN, NMTC1, MNG1 and TCO susceptibility loci and identification of somatic BRAF and RAS mutations." Endocr Relat Cancer **15**(1): 207-215.

Chan, J. K., M. S. Tsui and C. H. Tse (1987). "Diffuse sclerosing variant of papillary carcinoma of the thyroid: a histological and immunohistochemical study of three cases." Histopathology **11**(2): 191-201.

Chen, A. Y., A. Jemal and E. M. Ward (2009). "Increasing incidence of differentiated thyroid cancer in the United States, 1988-2005." Cancer **115**(16): 3801-3807.

Collini, P., F. Mattavelli, A. Pellegrinelli, M. Barisella, A. Ferrari and M. Massimino (2006). "Papillary carcinoma of the thyroid gland of childhood and adolescence: Morphologic subtypes, biologic behavior and prognosis: a clinicopathologic study of 42 sporadic cases treated at a single institution during a 30-year period." Am J Surg Pathol **30**(11): 1420-1426.



Crow, P., A. Molckovsky, N. Stone, J. Uff, B. Wilson and L. M. WongKeeSong (2005). "Assessment of fiberoptic near-infrared raman spectroscopy for diagnosis of bladder and prostate cancer." Urology **65**(6): 1126-1130.

Davies, L. and H. G. Welch (2014). "Current thyroid cancer trends in the United States." JAMA Otolaryngol Head Neck Surg **140**(4): 317-322.

Dean, D. S. and H. Gharib (2008). "Epidemiology of thyroid nodules." Best Pract Res Clin Endocrinol Metab **22**(6): 901-911.

DeLellis RA, Lloyd RV and H. PU (2004). Pathology and Genetics: Tumors of Endocrine Organs. Lyon, IARC Press.

di Masi, A., L. Leboffe, A. Sodo, G. Tabacco, R. Cesareo, M. Sbroscia, I. Giovannoni, C. Taffon, P. Crucitti, F. Longo, S. Manfrini, M. A. Ricci, P. Ascenzi, A. Crescenzi and A. Palermo (2019). "Metabolic profile of human parathyroid adenoma." Endocrine.

Duick, D. S., J. P. Kloppner, J. C. Diggans, L. Friedman, G. C. Kennedy, R. B. Lanman and B. McIver (2012). "The impact of benign gene expression classifier test results on the endocrinologist-patient decision to operate on patients with thyroid nodules with indeterminate fine-needle aspiration cytopathology." Thyroid **22**(10): 996-1001.

Duraipandian, S., W. Zheng, J. Ng, J. J. Low, A. Ilancheran and Z. Huang (2012). "Simultaneous fingerprint and high-wavenumber confocal Raman spectroscopy enhances early detection of cervical precancer in vivo." Anal Chem **84**(14): 5913-5919.

Elisei, R., B. Cosci, C. Romei, V. Bottici, G. Renzini, E. Molinaro, L. Agate, A. Vivaldi, P. Faviana, F. Basolo, P. Miccoli, P. Berti, F. Pacini and A. Pinchera (2008). "Prognostic significance of somatic RET oncogene mutations in sporadic medullary thyroid cancer: a 10-year follow-up study." J Clin Endocrinol Metab **93**(3): 682-687.



Eszlinger, M., K. Bohme, M. Ullmann, F. Gorke, U. Siebolts, A. Neumann, C. Franzius, S. Adam, T. Molwitz, C. Landvogt, B. Amro, A. Hach, B. Feldmann, D. Graf, A. Wefer, R. Niemann, C. Bullmann, G. Klausenke, R. Santen, G. Tonshoff, V. Ivancevic, A. Kogler, E. Bell, B. Lorenz, G. Kluge, C. Hartenstein, I. Ruschenburg and R. Paschke (2017). "Evaluation of a Two-Year Routine Application of Molecular Testing of Thyroid Fine-Needle Aspirations Using a Seven-Gene Panel in a Primary Referral Setting in Germany." Thyroid **27**(3): 402-411.

Etit, D., W. C. Faquin, R. Gaz, G. Randolph, R. A. DeLellis and B. Z. Pilch (2008). "Histopathologic and clinical features of medullary microcarcinoma and C-cell hyperplasia in prophylactic thyroidectomies for medullary carcinoma: a study of 42 cases." Arch Pathol Lab Med **132**(11): 1767-1773.

Frich, L., E. Glatre and L. A. Akslen (2001). "Familial occurrence of nonmedullary thyroid cancer: a population-based study of 5673 first-degree relatives of thyroid cancer patients from Norway." Cancer Epidemiol Biomarkers Prev **10**(2): 113-117.

Fukushima, M., Y. Ito, M. Hirokawa, H. Akasu, K. Shimizu and A. Miyauchi (2009). "Clinicopathologic characteristics and prognosis of diffuse sclerosing variant of papillary thyroid carcinoma in Japan: an 18-year experience at a single institution." World J Surg **33**(5): 958-962.

Gaffey, M. J., E. E. Lack, M. L. Christ and L. M. Weiss (1991). "Anaplastic thyroid carcinoma with osteoclast-like giant cells. A clinicopathologic, immunohistochemical, and ultrastructural study." Am J Surg Pathol **15**(2): 160-168.

Gharib, H., E. Papini, J. R. Garber, D. S. Duick, R. M. Harrell, L. Hegedus, R. Paschke, R. Valcavi, P. Vitti and A. A. A. T. F. o. T. Nodules (2016). "American Association of Clinical Endocrinologists, American College of Endocrinology, and Associazione Medici Endocrinologi Medical Guidelines for Clinical Practice for the Diagnosis and Management of Thyroid Nodules--2016 Update." Endocr Pract **22**(5): 622-639.



Giuffrida, D. and H. Gharib (1998). "Current diagnosis and management of medullary thyroid carcinoma." Ann Oncol **9**(7): 695-701.

Guth, S., U. Theune, J. Aberle, A. Galach and C. M. Bamberger (2009). "Very high prevalence of thyroid nodules detected by high frequency (13 MHz) ultrasound examination." Eur J Clin Invest **39**(8): 699-706.

Hanlon, E. B., R. Manoharan, T. W. Koo, K. E. Shafer, J. T. Motz, M. Fitzmaurice, J. R. Kramer, I. Itzkan, R. R. Dasari and M. S. Feld (2000). "Prospects for in vivo Raman spectroscopy." Phys Med Biol **45**(2): R1-59.

Hapke, M. R. and L. P. Dehner (1979). "The optically clear nucleus. A reliable sign of papillary carcinoma of the thyroid?" Am J Surg Pathol **3**(1): 31-38.

Harris, A. T., M. Garg, X. B. Yang, S. E. Fisher, J. Kirkham, D. A. Smith, D. P. Martin-Hirsch and A. S. High (2009). "Raman spectroscopy and advanced mathematical modelling in the discrimination of human thyroid cell lines." Head Neck Oncol **1**: 38.

Haugen, B. R., E. K. Alexander, K. C. Bible, G. M. Doherty, S. J. Mandel, Y. E. Nikiforov, F. Pacini, G. W. Randolph, A. M. Sawka, M. Schlumberger, K. G. Schuff, S. I. Sherman, J. A. Sosa, D. L. Steward, R. M. Tuttle and L. Wartofsky (2016). "2015 American Thyroid Association Management Guidelines for Adult Patients with Thyroid Nodules and Differentiated Thyroid Cancer: The American Thyroid Association Guidelines Task Force on Thyroid Nodules and Differentiated Thyroid Cancer." Thyroid **26**(1): 1-133.

He, H., R. Nagy, S. Liyanarachchi, H. Jiao, W. Li, S. Suster, J. Kere and A. de la Chapelle (2009). "A susceptibility locus for papillary thyroid carcinoma on chromosome 8q24." Cancer Res **69**(2): 625-631.

Hegedus, L. (2004). "Clinical practice. The thyroid nodule." N Engl J Med **351**(17): 1764-1771.



Hemminki, K., C. Eng and B. Chen (2005). "Familial risks for nonmedullary thyroid cancer." J Clin Endocrinol Metab **90**(10): 5747-5753.

Herrera, M. F., I. D. Hay, P. S. Wu, J. R. Goellner, J. J. Ryan, J. R. Ebersold, E. J. Bergstralh and C. S. Grant (1992). "Hurthle cell (oxyphilic) papillary thyroid carcinoma: a variant with more aggressive biologic behavior." World J Surg **16**(4): 669-674; discussion 774-665.

Hsiao, S. J. and Y. E. Nikiforov (2014). "Molecular approaches to thyroid cancer diagnosis." Endocr Relat Cancer **21**(5): T301-313.


Hundahl, S. A., I. D. Fleming, A. M. Fremgen and H. R. Menck (1998). "A National Cancer Data Base report on 53,856 cases of thyroid carcinoma treated in the U.S., 1985-1995 [see commetns]." Cancer **83**(12): 2638-2648.

Ito, Y., M. Hirokawa, T. Higashiyama, Y. Takamura, A. Miya, K. Kobayashi, F. Matsuzuka, K. Kuma and A. Miyauchi (2007). "Prognosis and prognostic factors of follicular carcinoma in Japan: importance of postoperative pathological examination." World J Surg **31**(7): 1417-1424.

Jermyn, M., K. Mok, J. Mercier, J. Desroches, J. Pichette, K. Saint-Arnaud, L. Bernstein, M. C. Guiot, K. Petrecca and F. Leblond (2015). "Intraoperative brain cancer detection with Raman spectroscopy in humans." Sci Transl Med **7**(274): 274ra219.

Jung, C. K., M. P. Little, J. H. Lubin, A. V. Brenner, S. A. Wells, Jr., A. J. Sigurdson and Y. E. Nikiforov (2014). "The increase in thyroid cancer incidence during the last four decades is accompanied by a high frequency of BRAF mutations and a sharp increase in RAS mutations." J Clin Endocrinol Metab **99**(2): E276-285.

Kallaway, C., L. M. Almond, H. Barr, J. Wood, J. Hutchings, C. Kendall and N. Stone (2013). "Advances in the clinical application of Raman spectroscopy for cancer diagnostics." Photodiagnosis Photodyn Ther **10**(3): 207-219.



Karabeber, H., R. Huang, P. Iacono, J. M. Samii, K. Pitter, E. C. Holland and M. F. Kircher (2014). "Guiding brain tumor resection using surface-enhanced Raman scattering nanoparticles and a hand-held Raman scanner." ACS Nano **8**(10): 9755-9766.

Kebebew, E., F. S. Greenspan, O. H. Clark, K. A. Woeber and A. McMillan (2005). "Anaplastic thyroid carcinoma. Treatment outcome and prognostic factors." Cancer **103**(7): 1330-1335.

Kendall, C., N. Stone, N. Shepherd, K. Geboes, B. Warren, R. Bennett and H. Barr (2003). "Raman spectroscopy, a potential tool for the objective identification and classification of neoplasia in Barrett's oesophagus." J Pathol **200**(5): 602-609.

Koljenovic, S., T. B. Schut, A. Vincent, J. M. Kros and G. J. Puppels (2005). "Detection of meningioma in dura mater by Raman spectroscopy." Anal Chem **77**(24): 7958-7965.

Kong, K., F. Zaabar, E. Rakha, I. Ellis, A. Koloydenko and I. Notingher (2014). "Towards intra-operative diagnosis of tumours during breast conserving surgery by selective-sampling Raman micro-spectroscopy." Phys Med Biol **59**(20): 6141-6152.

Layfield, L. J., T. Wax and C. Jones (2003). "Cytologic distinction of goiterous nodules from morphologically normal thyroid: analyses of cytomorphologic features." Cancer **99**(4): 217-222.

Leenhardt, L., M. O. Bernier, M. H. Boin-Pineau, B. Conte Devolx, R. Marechaud, P. Niccoli-Sire, M. Nocaudie, J. Orgiazzi, M. Schlumberger, J. L. Wemeau, L. Cherie-Challine and F. De Vathaire (2004). "Advances in diagnostic practices affect thyroid cancer incidence in France." Eur J Endocrinol **150**(2): 133-139.

Lithwick-Yanai, G., N. Dromi, A. Shtabsky, S. Morgenstern, Y. Strenov, M. Feinmesser, V. Kravtsov, M. E. Leon, M. Hajduch, S. Z. Ali, C. J. VandenBussche, X. Zhang, L. Leider-Trejo, A. Zubkov, S. Vorobyov, M. Kushnir, Y. Goren, S. Tabak, E. Kadosh, H. Benjamin, T. Schnitzer-Perlman, H. Marmor, M. Motin, D. Lebanony,



S. Kredon-Russo, H. Mitchell, M. Noller, A. Smith, O. Dattner, K. Ashkenazi, M. Sanden, K. A. Berlin, D. Bar and E. Meiri (2017). "Multicentre validation of a microRNA-based assay for diagnosing indeterminate thyroid nodules utilising fine needle aspirate smears." J Clin Pathol **70**(6): 500-507.

Liu, J., B. Singh, G. Tallini, D. L. Carlson, N. Katabi, A. Shaha, R. M. Tuttle and R. A. Ghossein (2006). "Follicular variant of papillary thyroid carcinoma: a clinicopathologic study of a problematic entity." Cancer **107**(6): 1255-1264.

LiVolsi, V. A. and S. L. Asa (1994). "The demise of follicular carcinoma of the thyroid gland." Thyroid **4**(2): 233-236.

Lopez-Penabad, L., A. C. Chiu, A. O. Hoff, P. Schultz, S. Gaztambide, N. G. Ordonez and S. I. Sherman (2003). "Prognostic factors in patients with Hurthle cell neoplasms of the thyroid." Cancer **97**(5): 1186-1194.

Lubitz, C. C., S. K. Ugras, J. J. Kazam, B. Zhu, T. Scognamiglio, Y. T. Chen and T. J. Fahey, 3rd (2006). "Microarray analysis of thyroid nodule fine-needle aspirates accurately classifies benign and malignant lesions." J Mol Diagn **8**(4): 490-498; quiz 528.

Mahadevan-Jansen, A. and R. R. Richards-Kortum (1996). "Raman spectroscopy for the detection of cancers and precancers." J Biomed Opt **1**(1): 31-70.

Malchoff, C. D., M. Sarfarazi, B. Tendler, F. Forouhar, G. Whalen, V. Joshi, A. Arnold and D. M. Malchoff (2000). "Papillary thyroid carcinoma associated with papillary renal neoplasia: genetic linkage analysis of a distinct heritable tumor syndrome." J Clin Endocrinol Metab **85**(5): 1758-1764.

Mandel, S. J. (2004). "A 64-year-old woman with a thyroid nodule." JAMA **292**(21): 2632-2642.



Marshall, C. P., S. Leuko, C. M. Coyle, M. R. Walter, B. P. Burns and B. A. Neilan (2007). "Carotenoid analysis of halophilic archaea by resonance Raman spectroscopy." Astrobiology **7**(4): 631-643.

Mazeh, H. and R. S. Sippel (2013). "Familial nonmedullary thyroid carcinoma." Thyroid **23**(9): 1049-1056.

Mazzanti, C., M. A. Zeiger, N. G. Costouros, C. Umbricht, W. H. Westra, D. Smith, H. Somervell, G. Bevilacqua, H. R. Alexander and S. K. Libutti (2004). "Using gene expression profiling to differentiate benign versus malignant thyroid tumors." Cancer Res **64**(8): 2898-2903.

Montgomery, E., M. P. Bronner, J. R. Goldblum, J. K. Greenson, M. M. Haber, J. Hart, L. W. Lamps, G. Y. Lauwers, A. J. Lazenby, D. N. Lewin, M. E. Robert, A. Y. Toledano, Y. Shyr and K. Washington (2001). "Reproducibility of the diagnosis of dysplasia in Barrett esophagus: a reaffirmation." Hum Pathol **32**(4): 368-378.

Nikiforov, Y. and D. R. Gnepp (1994). "Pediatric thyroid cancer after the Chernobyl disaster. Pathomorphologic study of 84 cases (1991-1992) from the Republic of Belarus." Cancer **74**(2): 748-766.

Nikiforov, Y., D. R. Gnepp and J. A. Fagin (1996). "Thyroid lesions in children and adolescents after the Chernobyl disaster: implications for the study of radiation tumorigenesis." J Clin Endocrinol Metab **81**(1): 9-14.

Nikiforov, Y. E., S. E. Carty, S. I. Chiosea, C. Coyne, U. Duvvuri, R. L. Ferris, W. E. Gooding, S. P. Hodak, S. O. LeBeau, N. P. Ohori, R. R. Seethala, M. E. Tublin, L. Yip and M. N. Nikiforova (2014). "Highly accurate diagnosis of cancer in thyroid nodules with follicular neoplasm/suspicious for a follicular neoplasm cytology by ThyroSeq v2 next-generation sequencing assay." Cancer **120**(23): 3627-3634.

Nikiforov, Y. E., S. E. Carty, S. I. Chiosea, C. Coyne, U. Duvvuri, R. L. Ferris, W. E. Gooding, S. O. LeBeau, N. P. Ohori, R. R. Seethala, M. E. Tublin, L. Yip and M. N. Nikiforova (2015). "Impact of the Multi-Gene ThyroSeq Next-Generation Sequencing



Assay on Cancer Diagnosis in Thyroid Nodules with Atypia of Undetermined Significance/Follicular Lesion of Undetermined Significance Cytology." Thyroid **25**(11): 1217-1223.

Nikiforov, Y. E., N. P. Ohori, S. P. Hodak, S. E. Carty, S. O. LeBeau, R. L. Ferris, L. Yip, R. R. Seethala, M. E. Tublin, M. T. Stang, C. Coyne, J. T. Johnson, A. F. Stewart and M. N. Nikiforova (2011). "Impact of mutational testing on the diagnosis and management of patients with cytologically indeterminate thyroid nodules: a prospective analysis of 1056 FNA samples." J Clin Endocrinol Metab **96**(11): 3390-3397.

Nikiforov, Y. E., D. L. Steward, T. M. Robinson-Smith, B. R. Haugen, J. P. Klopper, Z. Zhu, J. A. Fagin, M. Falciglia, K. Weber and M. N. Nikiforova (2009). "Molecular testing for mutations in improving the fine-needle aspiration diagnosis of thyroid nodules." J Clin Endocrinol Metab **94**(6): 2092-2098.

Nikiforova, M. N., A. I. Wald, S. Roy, M. B. Durso and Y. E. Nikiforov (2013). "Targeted next-generation sequencing panel (ThyroSeq) for detection of mutations in thyroid cancer." J Clin Endocrinol Metab **98**(11): E1852-1860.

O'Grady, T. J., M. A. Gates and F. P. Boscoe (2015). "Thyroid cancer incidence attributable to overdiagnosis in the United States 1981-2011." Int J Cancer **137**(11): 2664-2673.

Pacini, F., M. Schlumberger, H. Dralle, R. Elisei, J. W. Smit, W. Wiersinga and T. European Thyroid Cancer (2006). "European consensus for the management of patients with differentiated thyroid carcinoma of the follicular epithelium." Eur J Endocrinol **154**(6): 787-803.

Pagan, M., R. T. Kloos, C. F. Lin, K. J. Travers, H. Matsuzaki, E. Y. Tom, S. Y. Kim, M. G. Wong, A. C. Stewart, J. Huang, P. S. Walsh, R. J. Monroe and G. C. Kennedy (2016). "The diagnostic application of RNA sequencing in patients with thyroid



cancer: an analysis of 851 variants and 133 fusions in 524 genes." BMC Bioinformatics **17 Suppl 1**: 6.

Pereira, T. M., D. M. Zezell, B. Bird, M. Miljkovic and M. Diem (2013). "The characterization of normal thyroid tissue by micro-FTIR spectroscopy." Analyst **138**(23): 7094-7100.

Perumal, J., G. Balasundaram, A. P. Mahyuddin, M. Choolani and M. Olivo (2015). "SERS-based quantitative detection of ovarian cancer prognostic factor haptoglobin." Int J Nanomedicine **10**: 1831-1840.

Prasad, N. B., H. Somervell, R. P. Tufano, A. P. Dackiw, M. R. Marohn, J. A. Califano, Y. Wang, W. H. Westra, D. P. Clark, C. B. Umbricht, S. K. Libutti and M. A. Zeiger (2008). "Identification of genes differentially expressed in benign versus malignant thyroid tumors." Clin Cancer Res **14**(11): 3327-3337.

Puppels, G. J., H. S. Garritsen, J. A. Kummer and J. Greve (1993). "Carotenoids located in human lymphocyte subpopulations and natural killer cells by Raman microspectroscopy." Cytometry **14**(3): 251-256.

Rau, J. V., M. Fosca, V. Graziani, C. Taffon, M. Rocchia, M. Caricato, P. Pozzilli, A. Onetti Muda and A. Crescenzi (2017). "Proof-of-concept Raman spectroscopy study aimed to differentiate thyroid follicular patterned lesions." Sci Rep **7**(1): 14970.

Rau, J. V., V. Graziani, M. Fosca, C. Taffon, M. Rocchia, P. Crucitti, P. Pozzilli, A. Onetti Muda, M. Caricato and A. Crescenzi (2016). "RAMAN spectroscopy imaging improves the diagnosis of papillary thyroid carcinoma." Sci Rep **6**: 35117.

Roth, M. Y., R. L. Witt and D. L. Steward (2018). "Molecular testing for thyroid nodules: Review and current state." Cancer **124**(5): 888-898.

Rout, P. and S. Shariff (1999). "Diagnostic value of qualitative and quantitative variables in thyroid lesions." Cytopathology **10**(3): 171-179.



Schmid, D., C. Ricci, G. Behrens and M. F. Leitzmann (2015). "Adiposity and risk of thyroid cancer: a systematic review and meta-analysis." Obes Rev **16**(12): 1042-1054.

Scopa, C. D., M. Melachrinou, C. Saradopoulou and M. J. Merino (1993). "The significance of the grooved nucleus in thyroid lesions." Mod Pathol **6**(6): 691-694.

Shaha, A. R., T. R. Loree and J. P. Shah (1995). "Prognostic factors and risk group analysis in follicular carcinoma of the thyroid." Surgery **118**(6): 1131-1136; discussion 1136-1138.

Sherman, S. I. (2003). "Thyroid carcinoma." Lancet **361**(9356): 501-511.

Siegel, R. L., K. D. Miller and A. Jemal (2016). "Cancer statistics, 2016." CA Cancer J Clin **66**(1): 7-30.


Smith-Bindman, R., P. Lebda, V. A. Feldstein, D. Sellami, R. B. Goldstein, N. Brasic, C. Jin and J. Kornak (2013). "Risk of thyroid cancer based on thyroid ultrasound imaging characteristics: results of a population-based study." JAMA Intern Med **173**(19): 1788-1796.

Stojadinovic, A., R. A. Ghossein, A. Hoos, M. J. Urist, R. H. Spiro, J. P. Shah, M. F. Brennan, A. R. Shaha and B. Singh (2001). "Hurthle cell carcinoma: a critical histopathologic appraisal." J Clin Oncol **19**(10): 2616-2625.

Stone, N., R. Baker, K. Rogers, A. W. Parker and P. Matousek (2007). "Subsurface probing of calcifications with spatially offset Raman spectroscopy (SORS): future possibilities for the diagnosis of breast cancer." Analyst **132**(9): 899-905.

Stone, N. and P. Matousek (2008). "Advanced transmission Raman spectroscopy: a promising tool for breast disease diagnosis." Cancer Res **68**(11): 4424-4430.

Stone, N., P. Stavroulaki, C. Kendall, M. Birchall and H. Barr (2000). "Raman spectroscopy for early detection of laryngeal malignancy: preliminary results." Laryngoscope **110**(10 Pt 1): 1756-1763.



Sugino, K., K. Ito, T. Mimura, K. Kameyama, H. Iwasaki and K. Ito (2001). "Hurthle cell tumor of the thyroid: analysis of 188 cases." World J Surg **25**(9): 1160-1163.

Sugitani, I., Y. Hasegawa, M. Sugasawa, M. Tori, T. Higashiyama, M. Miyazaki, H. Hosoi, Y. Orita and H. Kitano (2014). "Super-radical surgery for anaplastic thyroid carcinoma: a large cohort study using the Anaplastic Thyroid Carcinoma Research Consortium of Japan database." Head Neck **36**(3): 328-333.

Talari, A. C. S., Z. Movasaghi, S. Rehman and I. u. Rehman (2015). "Raman Spectroscopy of Biological Tissues." Applied Spectroscopy Reviews **50**(1): 46-111.

Tan, G. H. and H. Gharib (1997). "Thyroid incidentalomas: management approaches to nonpalpable nodules discovered incidentally on thyroid imaging." Ann Intern Med **126**(3): 226-231.

Teixeira, C. S., R. A. Bitar, H. S. Martinho, A. B. Santos, M. A. Kulcsar, C. U. Friguglietti, R. B. da Costa, E. A. Arisawa and A. A. Martin (2009). "Thyroid tissue analysis through Raman spectroscopy." Analyst **134**(11): 2361-2370.

Tessler, F. N., W. D. Middleton, E. G. Grant, J. K. Hoang, L. L. Berland, S. A. Teefey, J. J. Cronan, M. D. Beland, T. S. Desser, M. C. Frates, L. W. Hammers, U. M. Hamper, J. E. Langer, C. C. Reading, L. M. Scoutt and A. T. Stavros (2017). "ACR Thyroid Imaging, Reporting and Data System (TI-RADS): White Paper of the ACR TI-RADS Committee." J Am Coll Radiol **14**(5): 587-595.

Tielens, E. T., S. I. Sherman, R. H. Hruban and P. W. Ladenson (1994). "Follicular variant of papillary thyroid carcinoma. A clinicopathologic study." Cancer **73**(2): 424-431.

Tomaz, R. A., I. Sousa, J. G. Silva, C. Santos, M. R. Teixeira, V. Leite and B. M. Cavaco (2012). "FOXE1 polymorphisms are associated with familial and sporadic nonmedullary thyroid cancer susceptibility." Clin Endocrinol (Oxf) **77**(6): 926-933.



Tronko, M. D., T. I. Bogdanova, I. V. Komissarenko, O. V. Epstein, V. Oliynyk, A. Kovalenko, I. A. Likhtarev, I. Kairo, S. B. Peters and V. A. LiVolsi (1999). "Thyroid carcinoma in children and adolescents in Ukraine after the Chernobyl nuclear accident: statistical data and clinicomorphologic characteristics." Cancer **86**(1): 149-156.

Tunbridge, W. M., D. C. Evered, R. Hall, D. Appleton, M. Brewis, F. Clark, J. G. Evans, E. Young, T. Bird and P. A. Smith (1977). "The spectrum of thyroid disease in a community: the Whickham survey." Clin Endocrinol (Oxf) **7**(6): 481-493.

Untch, B. R. and J. A. Olson, Jr. (2006). "Anaplastic thyroid carcinoma, thyroid lymphoma, and metastasis to thyroid." Surg Oncol Clin N Am **15**(3): 661-679, x.


Upchurch, E., M. Isabelle, G. R. Lloyd, C. Kendall and H. Barr (2018). "An update on the use of Raman spectroscopy in molecular cancer diagnostics: current challenges and further prospects." Expert Rev Mol Diagn **18**(3): 245-258.

Valderrabano, P., L. Khazai, M. E. Leon, Z. J. Thompson, Z. Ma, C. H. Chung, J. E. Hallanger-Johnson, K. J. Otto, K. D. Rogers, B. A. Centeno and B. McIver (2017). "Evaluation of ThyroSeq v2 performance in thyroid nodules with indeterminate cytology." Endocr Relat Cancer **24**(3): 127-136.

van Heerden, J. A., I. D. Hay, J. R. Goellner, D. Salomao, J. R. Ebersold, E. J. Bergstralh and C. S. Grant (1992). "Follicular thyroid carcinoma with capsular invasion alone: a nonthreatening malignancy." Surgery **112**(6): 1130-1136; discussion 1136-1138.

Vander, J. B., E. A. Gaston and T. R. Dawber (1968). "The significance of nontoxic thyroid nodules. Final report of a 15-year study of the incidence of thyroid malignancy." Ann Intern Med **69**(3): 537-540.

Wu, L., Z. Wang, S. Zong, H. Chen, C. Wang, S. Xu and Y. Cui (2013). "Simultaneous evaluation of p53 and p21 expression level for early cancer diagnosis using SERS technique." Analyst **138**(12): 3450-3456.



Zhang, J. Q., Y. S. Wang, Y. He, T. Jiang, H. M. Yang, X. Tan, R. H. Kang, Y. K. Yuan and L. F. Shi (2010). "Determination of urinary adenosine using resonance light scattering of gold nanoparticles modified structure-switching aptamer." Anal Biochem **397**(2): 212-217.

